NR*xx* Simulation of Microflows with Shakhov Model

Zhenning Cai[*],   Ruo Li[†],   Zhonghua Qiao[‡]

September 4, 2018

Abstract

In this paper, we propose a method to simulate the microflows with Shakhov model using the NR*xx* method developed in [4, 6, 5]. The equation under consideration is the Boltzmann equation with force terms and the Shakhov model is adopted to achieve the correct Prandtl number. As the focus of this paper, we derive a uniform framework for different order moment systems on the wall boundary conditions, which is a major difficulty in the moment methods. Numerical examples for both steady and unsteady problems are presented to show the convergence in the number of moments.

Keywords: NR*xx* method, Shakhov model, boundary conditions, microflow

1 Introduction

In the kinetic theory, the degree of rarefaction of a gas is often characterized by the dimensionless Knudsen number $Kn = \lambda/L$, where λ is the mean free path and L is the relevant characteristic length. The classic Navier-Stokes-Fourier (NSF) equations are accurate only when $Kn < 0.01$. However, the ongoing miniaturization of technical devices requires modelling of gas in microscopic channels, for which the characteristic length L is so small that even under normal density and temperature, the Knudsen number is beyond the available region of NSF equations. Meanwhile, in the transitional regime $(0.1 < Kn < 10)$, the traditional no-slip wall boundary condition is no longer valid. In order to match the physical experimentation, the interaction between wall and gas should be carefully conducted. We refer the readers to [13] for more details.

For microflows, it is known that the Boltzmann equation with Maxwell boundary conditions [15] is able to accurately describe the flow state. However, on the computational perspective, the cost for solving Boltzmann equation directly is unacceptable in the general case. Grad [7] did a pioneer work which extends Euler equations to a thirteen-moment system, which opened a new way for modelling rarefied gas flow called as moment method. However, it was discovered by Grad himself in [8] that this system fails to give smooth shock profiles when the Mach number is larger than 1.65. To remedy this drawback, some authors tend to construct a parabolic system similar to the NSF equations. In this field, some methods such as Jin-Slemrod [12], COET [17] and R13 [9, 24] were subsequently raised. Concurrently, increasing attention is attracted to systems with more than 13

---

[*]School of Mathematical Sciences, Peking University, Beijing, China, email: `caizn@pku.edu.cn`.

[†]CAPT, LMAM & School of Mathematical Sciences, Peking University, Beijing, China, email: `rli@math.pku.edu.cn`.

[‡]Institute for Computational Mathematics & Department of Mathematics, Hong Kong Baptist University, Kowloon Tong, Hong Kong, email: `zqiao@hkbu.edu.hk`.

moments (e.g. [29, 21]). As a combination of these two directions, R20 and R26 equations were respectively studied in [16] and [11]. In [4], a general method for numerically solving the regularized moment equations of arbitrary order was proposed, and it was improved in [5, 6] and abbreviated as NRxx method in [6] for convenience. On the other hand, the boundary condition for the moment methods is a major obstacle for applications of moment methods in the field of microflows. In Grad's paper [7], the basic idea for the modelling of Maxwell boundary conditions in the framework of moment method is raised. The idea was also used in [28, 11] for R13 and R26 equations. However, for general moment equations, the numerical method to process the boundary conditions for NRxx method is unavailable yet.

The major concern of this paper is to supply suitable boundary conditions for NRxx method. Before that, the NRxx method is first improved such that it is able to predict stress and heat flux correctly in the dense case. This is achieved by replacing the BGK collision model [2] used in [4, 5, 6] with the Shakhov model [19]. Recall that for the BGK model, collision term can be analytically solved when using the NRxx method. Similarly, analytical solution for each moment can also be obtained when using the Shakhov model. At the same time, the force term is also applied to the NRxx method, and one can find that this term only affects the momentum equation that it is turned to be trivial when splitting method is employed.

As to the wall boundary conditions, we follow the idea of Grad [7] and try to approximate Maxwell boundary condition using moment method. The Maxwell boundary condition is a linear combination of specular reflection and diffusive reflection. According to Grad's theory, only the moments of odd order in the normal microscopic velocity are controlled by boundary conditions. These moments for the specularly reflective part vanish. For the diffusive reflection, the incidence part and the emergence part are considered separately. For the incidence part, one need to calculate the moments of a distribution cut off by a half space. Since the distribution is expressed by a finite expansion of Hermite series, the cut-off turns out to be quite intricate. We eventually derive a simple recursive formula to obtain these moments with careful investigation into the detailed expressions. The obtained formula brings only slight increment of the computational cost. For the emergence part, which is a half Maxwellian, the moments are obtained by direct integration, and the result is also given in a recursive form. The overall boundary condition is the summation of both the specular part and diffusive part, which is rearranged into a simple formulation. It is numerically implemented by first constructing a set of moments satisfying the boundary conditions, and then approximating the flow state in the ghost cell with a first order extrapolation of each moment. Thus, boundary conditions for the NRxx method of all orders are collected into a uniform framework, which avoids separate and involved implementation for different systems with sophisticated expressions [26, 28, 11].

A number of numerical examples are presented to show the validity of the boundary conditions. Both steady and unsteady problems are studied. Numerical simulations up to 455-moment system are carried out. The classic symmetric planar Couette flow and force-driven Poiseuille flow are investigated as examples for steady problems. All the numerical results exhibit the convergence of the NRxx method as the number of moments increases.

The layout of this paper is as follows: in Section 2, we give a brief introduction to the Boltzmann equation and the NRxx method. In Section 3, the Shakhov collision model and the force-induced acceleration terms are coupled with the NRxx method. In Section 4, the derivation of boundary conditions are carried out. Numerical examples are shown in Section 5, and some discussions on the validity and accuracy of the NRxx method are

2

given in Section 6. Finally, we make some conclusion in Section 7.

2   The Boltzmann equation and the NRxx method

The Boltzmann equation is the basic equation in the kinetic theory, where a distribution function $f(t, \boldsymbol{x}, \boldsymbol{\xi})$ is introduced to provide a statistical description for the motion of molecules. Here $t \in \mathbb{R}^+$ is the time, and $\boldsymbol{x}, \boldsymbol{\xi} \in \mathbb{R}^3$ are the position and velocity of particles. The Boltzmann equation reads

$$\frac{\partial f}{\partial t} + \boldsymbol{\xi} \cdot \nabla_{\boldsymbol{x}} f + \boldsymbol{F} \cdot \nabla_{\boldsymbol{\xi}} f = Q(f, f), \tag{2.1}$$

where $\boldsymbol{F}$ is the acceleration of particles caused by external forces. The detailed expression of the collision term $Q(f, f)$ is not presented here due to its complexity, but we stress that $Q(f, f)$ contains a five-dimensional integration which causes great difficulty in the numerical simulation. Instead, simplified collision models such as the BGK model [2] and the Shakhov model [19] are adopted in this paper. These models read:

1. *BGK model:*

$$\frac{\partial f}{\partial t} + \boldsymbol{\xi} \cdot \nabla_{\boldsymbol{x}} f + \boldsymbol{F} \cdot \nabla_{\boldsymbol{\xi}} f = \frac{1}{\tau}(f_M - f); \tag{2.2}$$

2. *Shakhov model:*

$$\frac{\partial f}{\partial t} + \boldsymbol{\xi} \cdot \nabla_{\boldsymbol{x}} f + \boldsymbol{F} \cdot \nabla_{\boldsymbol{\xi}} f = \frac{1}{\tau} \left\{ \left[1 + \frac{(1 - \mathrm{Pr})(\boldsymbol{\xi} - \boldsymbol{u}) \cdot \boldsymbol{q}}{5\rho\theta^2} \left(\frac{|\boldsymbol{\xi} - \boldsymbol{u}|^2}{\theta} - 5 \right) \right] f_M - f \right\}. \tag{2.3}$$

Here ρ, $\boldsymbol{u}$, θ and $\boldsymbol{q}$ denote the density, mean velocity, temperature and heat flux respectively, and these macroscopic variables are related with the distribution function f by

$$\rho = \int_{\mathbb{R}^3} f \, \mathrm{d}\boldsymbol{\xi}, \quad \boldsymbol{u} = \frac{1}{\rho} \int_{\mathbb{R}^3} \boldsymbol{\xi} f \, \mathrm{d}\boldsymbol{\xi},$$
$$\theta = \frac{1}{3\rho} \int_{\mathbb{R}^3} |\boldsymbol{\xi} - \boldsymbol{u}|^2 f \, \mathrm{d}\boldsymbol{\xi}, \quad \boldsymbol{q} = \frac{1}{2} \int_{\mathbb{R}^3} |\boldsymbol{\xi} - \boldsymbol{u}|^2 (\boldsymbol{\xi} - \boldsymbol{u}) f \, \mathrm{d}\boldsymbol{\xi}. \tag{2.4}$$

Besides, τ is the relaxation time and f_M is the local Maxwellian which can be analytically formulated by

$$f_M = \frac{\rho}{(2\pi\theta)^{3/2}} \exp\left(-\frac{|\boldsymbol{\xi} - \boldsymbol{u}|^2}{2\theta} \right). \tag{2.5}$$

In (2.3), Pr stands for the Prandtl number which is a constant. One can easily observe that if Pr = 1, then the Shakhov model reduces to the BGK model, which agrees with the common knowledge that the BGK model predicts an incorrect Prandtl number 1.

The NRxx method is a numerical tool for solving large moment equations. It originated in [4] and was simplified in [5]. The basic idea is to expand the distribution function f into the Hermite series:

$$f(t, \boldsymbol{x}, \boldsymbol{\xi}) = \sum_{\alpha \in \mathbb{N}^3} f_\alpha(t, \boldsymbol{x}) \mathcal{H}_{\theta, \alpha} \left(\frac{\boldsymbol{\xi} - \boldsymbol{u}(t, \boldsymbol{x})}{\sqrt{\theta(t, \boldsymbol{x})}} \right), \tag{2.6}$$

3

where $\mathcal{H}_{\theta,\alpha}$ is the basis function defined as

$$\mathcal{H}_{\theta,\alpha}(\boldsymbol{v}) = \prod_{d=1}^{3} \frac{1}{\sqrt{2\pi}} \theta^{-\frac{\alpha_d+1}{2}} He_{\alpha_d}(v_d) \exp\left(-\frac{v_d^2}{2}\right), \quad \forall \alpha \in \mathbb{N}^3, \tag{2.7}$$

and He_n is the Hermite polynomials

$$He_n(x) = (-1)^n \exp\left(\frac{x^2}{2}\right) \frac{\mathrm{d}^n}{\mathrm{d}x^n} \exp\left(-\frac{x^2}{2}\right). \tag{2.8}$$

For convenience, we let $He_n(x) \equiv 0$ if $n < 0$. Thus $\mathcal{H}_{\theta,\alpha}(\boldsymbol{v})$ is zero when any of the components of α is negative.

With the expansion (2.6), the coefficients f_α can be considered as a set of infinite moments, and we have the following relations:

$$f_0 = \rho, \quad f_{e_i} = 0, \quad \sum_{d=1}^{3} f_{2e_d} = 0,$$

$$\sigma_{ij} = f_{e_i+e_j}, \quad \sigma_{ii} = 2f_{2e_i}, \quad q_i = 2f_{3e_i} + \sum_{d=1}^{3} f_{2e_d+e_i}, \tag{2.9}$$

where $i,j = 1,2,3$ and $i \neq j$, and σ_{ij} is the stress tensor or pressure deviators, which can be deduced from the distribution function f by

$$\sigma_{ij} = p_{ij} - \frac{1}{3}\delta_{ij}\sum_{d=1}^{3} p_{dd}, \quad \text{with} \quad p_{ij} = \int_{\mathbb{R}^3} (\xi_i - u_i)(\xi_j - u_j) f \,\mathrm{d}\boldsymbol{\xi}, \qquad i,j = 1,2,3. \tag{2.10}$$

In order to implement (2.6) numerically, a positive integer $M \geqslant 3$ is chosen and only the coefficients $\{f_\alpha(t,\boldsymbol{x})\}_{|\alpha|\leqslant M}$ are stored. Due to the absence of higher order moments, the resulting moment system is not closed. According to [5], the $(M+1)$-st order moments are approximated by

$$f_\alpha = \tau\left\{ \frac{1}{\rho}\sum_{j=1}^{D} \frac{\partial(\rho\theta)}{\partial x_j} f_{\alpha-e_j} + \frac{\theta}{D}\left(\sum_{j=1}^{D} \frac{\partial u_j}{\partial x_j}\right)\sum_{d=1}^{D} f_{\alpha-2e_d} - \sum_{j=1}^{D}\left[\theta\frac{\partial f_{\alpha-e_j}}{\partial x_j} \right.\right.$$

$$\left.\left. + \sum_{d=1}^{D}\left(\frac{\partial u_d}{\partial x_j}\theta f_{\alpha-e_d-e_j} + \frac{1}{2}\frac{\partial\theta}{\partial x_j}(\theta f_{\alpha-2e_d-e_j} + (\alpha_j+1)f_{\alpha-2e_d+e_j})\right)\right]\right\}. \tag{2.11}$$

Here f_α is taken as zero when any of α's components is negative. The numerical scheme for the force-free BGK model has been constructed in [6] based on the finite volume scheme with linear reconstruction and the fractional step method. Suppose the problem is in 1D and the grid is uniform with cell size Δx. We denote the cell centers as x_j, and then a full time step of the scheme can be sketched as follows:

1. Determine the time step size Δt.

2. Reconstruct the first M-th order moments for the distribution functions on cell boundaries $x_{j\pm1/2}$ with a conservative linear reconstruction.

3. Get the $(M+1)$-st order moments for the distribution functions on cell boundaries with a direct discretization of (2.11).

4. Apply the HLL scheme to solve the purely advective equation $\partial_t f + \boldsymbol{\xi} \cdot \nabla_{\boldsymbol{x}} f = 0$ over a time step of length Δt.

5. Analytically solve the pure collision equation of the BGK model $\partial_t f = (f_M - f)/\tau$ over a time step of length Δt.

We refer the readers to [4, 5, 6] for details of the algorithm. Here we only note that the Step 4 is nontrivial since two distributions cannot be added up directly, and in Step 5, the reason why the collision-only equation can be directly solved is that f_M can be expressed in the Hermite series $\{\mathcal{H}_{\theta,\alpha}\}$ trivially as $f_M = f_0 \mathcal{H}_{\theta,0}\left((\boldsymbol{\xi} - \boldsymbol{u})/\sqrt{\theta}\right)$.

3   The NRxx method for Shakhov model with force terms

As is well known, the Prandtl number for monatomic gases is around 2/3, while the BGK model gives a Prandtl number 1, which causes incorrect prediction of the stress tensor σ_{ij} or heat flux $\boldsymbol{q}$ for a dense gas. As a remedy, the Shakhov model was introduced in [19] as a generalization of the BGK model. The difference between these two models has been investigated in [31, 14]. In this section, we extend the NRxx method in [5] to the Shakhov model, and the force terms in (2.3) is added.

3.1   The governing equations

The moment system for the Shakhov model (2.3) with moment set $\{f_\alpha(t, \boldsymbol{x})\}_{|\alpha| \leqslant M}$ will be deduced here. As in [5], the strategy is to expand (2.3) into Hermite series, and then match the coefficients for the same basis functions. In order to simplify the notation, we define

$$
\begin{aligned}
A &= \frac{\partial f}{\partial t} + \boldsymbol{\xi} \cdot \nabla_{\boldsymbol{x}} f, \\
B &= \boldsymbol{F} \cdot \nabla_{\boldsymbol{\xi}} f, \\
C &= \frac{1}{\tau}\left\{\left[1 + \frac{(1-\mathrm{Pr})(\boldsymbol{\xi} - \boldsymbol{u}) \cdot \boldsymbol{q}}{5\rho\theta^2}\left(\frac{|\boldsymbol{\xi} - \boldsymbol{u}|^2}{\theta} - 5\right)\right] f_M - f\right\}.
\end{aligned}
\tag{3.1}
$$

It has been deduced in [5] that the Hermite expansion of A is

$$
\begin{aligned}
A = \sum_{\alpha \in \mathbb{N}^3} &\left\{\left(\frac{\partial f_\alpha}{\partial t} + \sum_{d=1}^{3} \frac{\partial u_d}{\partial t} f_{\alpha - e_d} + \frac{1}{2} \frac{\partial \theta}{\partial t} \sum_{d=1}^{3} f_{\alpha - 2e_d}\right)\right. \\
&+ \sum_{j=1}^{3}\left[\left(\theta \frac{\partial f_{\alpha - e_j}}{\partial x_j} + u_j \frac{\partial f_\alpha}{\partial x_j} + (\alpha_j + 1)\frac{\partial f_{\alpha + e_j}}{\partial x_j}\right)\right. \\
&+ \sum_{d=1}^{3} \frac{\partial u_d}{\partial x_j}\left(\theta f_{\alpha - e_d - e_j} + u_j f_{\alpha - e_d} + (\alpha_j + 1)f_{\alpha - e_d + e_j}\right) \\
&\left.\left. + \frac{1}{2} \frac{\partial \theta}{\partial x_j} \sum_{d=1}^{3}\left(\theta f_{\alpha - 2e_d - e_j} + u_j f_{\alpha - 2e_d} + (\alpha_j + 1)f_{\alpha - 2e_d + e_j}\right)\right]\right\} \mathcal{H}_{\theta,\alpha}\left(\frac{\boldsymbol{\xi} - \boldsymbol{u}}{\sqrt{\theta}}\right).
\end{aligned}
\tag{3.2}
$$

Using the differential relation of the Hermite polynomials, we have

$$
\frac{\partial}{\partial \xi_d} \mathcal{H}_{\theta,\alpha}\left(\frac{\boldsymbol{\xi} - \boldsymbol{u}}{\sqrt{\theta}}\right) = -\mathcal{H}_{\theta,\alpha + e_d}\left(\frac{\boldsymbol{\xi} - \boldsymbol{u}}{\sqrt{\theta}}\right).
\tag{3.3}
$$

Thus the Hermite expansion of the force term B can be easily deduced as

$$B = -\sum_{\alpha \in \mathbb{N}^3} \sum_{d=1}^{3} F_d f_{\alpha - e_d} \mathcal{H}_{\theta, \alpha} \left(\frac{\boldsymbol{\xi} - \boldsymbol{u}}{\sqrt{\theta}} \right). \tag{3.4}$$

The expansion of the collision term C can also be obtained by direct calculation. The result is

$$C = \frac{1}{\tau} \left[\frac{1 - \mathrm{Pr}}{5} \sum_{i=1}^{3} \sum_{j=1}^{3} q_i \mathcal{H}_{\theta, e_i + 2e_j} \left(\frac{\boldsymbol{\xi} - \boldsymbol{u}}{\sqrt{\theta}} \right) - \sum_{|\alpha| \geqslant 2} f_\alpha \mathcal{H}_{\theta, \alpha} \left(\frac{\boldsymbol{\xi} - \boldsymbol{u}}{\sqrt{\theta}} \right) \right]. \tag{3.5}$$

Putting (3.2)(3.4) and (3.5) into the Boltzmann-Shakhov equation $A + B = C$ and extracting coefficients for all basis functions, with a slight rearrangement, we get the following general moment equations for Shakhov model:

$$\frac{\partial f_\alpha}{\partial t} + \sum_{d=1}^{3} \left(\frac{\partial u_d}{\partial t} + \sum_{j=1}^{3} u_j \frac{\partial u_d}{\partial x_j} - F_d \right) f_{\alpha - e_d} + \frac{1}{2} \left(\frac{\partial \theta}{\partial t} + \sum_{j=1}^{3} u_j \frac{\partial \theta}{\partial x_j} \right) \sum_{d=1}^{3} f_{\alpha - 2e_d}$$

$$+ \sum_{j,d=1}^{3} \left[\frac{\partial u_d}{\partial x_j} \left(\theta f_{\alpha - e_d - e_j} + (\alpha_j + 1) f_{\alpha - e_d + e_j} \right) + \frac{1}{2} \frac{\partial \theta}{\partial x_j} \left(\theta f_{\alpha - 2e_d - e_j} + (\alpha_j + 1) f_{\alpha - 2e_d + e_j} \right) \right]$$

$$+ \sum_{j=1}^{3} \left(\theta \frac{\partial f_{\alpha - e_j}}{\partial x_j} + u_j \frac{\partial f_\alpha}{\partial x_j} + (\alpha_j + 1) \frac{\partial f_{\alpha + e_j}}{\partial x_j} \right) = \frac{1}{\tau} \left(\frac{1 - \mathrm{Pr}}{5} \sum_{i,j=1}^{3} \delta_{ij}(\alpha) q_i - \delta(\alpha) f_\alpha \right),$$

$$\tag{3.6}$$

where $\delta_{ij}(\alpha)$ and $\delta(\alpha)$ are defined by

$$\delta_{ij}(\alpha) = \begin{cases} 1, & \text{if } \alpha = e_i + 2e_j, \\ 0, & \text{otherwise,} \end{cases} \qquad \delta(\alpha) = \begin{cases} 1, & \text{if } |\alpha| \geq 2, \\ 0, & \text{otherwise.} \end{cases} \tag{3.7}$$

Now we will explore something more from (3.6). Noting that $f_{e_j} = 0$, $\forall j = 1, 2, 3$, the following relation can be obtained if we put $\alpha = 0$ into (3.6):

$$\frac{\partial f_0}{\partial x_j} + \sum_{j=1}^{3} \left(u_j \frac{\partial f_0}{\partial x_j} + f_0 \frac{\partial u_j}{\partial x_j} \right) = 0. \tag{3.8}$$

This is the mass conservation law. If we set $\alpha = e_d$, $d = 1, 2, 3$, the equations are

$$f_0 \left(\frac{\partial u_d}{\partial t} + \sum_{j=1}^{3} u_j \frac{\partial u_d}{\partial x_j} - F_d \right) + f_0 \frac{\partial \theta}{\partial x_d} + \theta \frac{\partial f_0}{\partial x_d} + \sum_{j=1}^{3} (\delta_{jd} + 1) \frac{\partial f_{e_d + e_j}}{\partial x_j} = 0. \tag{3.9}$$

This equation can be simplified as

$$f_0 \left(\frac{\partial u_d}{\partial t} + \sum_{j=1}^{3} u_j \frac{\partial u_d}{\partial x_j} - F_d \right) + \sum_{j=1}^{3} \frac{\partial p_{jd}}{\partial x_j} = 0. \tag{3.10}$$

Now we consider the case of $|\alpha| \geqslant 2$. Substituting (3.10) into (3.6), the temporal differentiation of $\boldsymbol{u}$ can be eliminated. In order to eliminate the temporal differentiation of θ, we

6

multiply (2.3) by $|\boldsymbol{\xi} - \boldsymbol{u}|^2$ on both sides and then integrate on $\mathbb{R}^3$ with respect to $\boldsymbol{\xi}$. The result is

$$f_0 \left(\frac{\partial \theta}{\partial t} + \sum_{j=1}^{3} u_j \frac{\partial \theta}{\partial x_j} \right) + \frac{2}{3} \sum_{j=1}^{3} \left(\frac{\partial q_j}{\partial x_j} + \sum_{d=1}^{3} p_{jd} \frac{\partial u_d}{\partial x_j} \right) = 0. \tag{3.11}$$

Note that the force term does not appear in this equation, since

$$\int_{\mathbb{R}^3} |\boldsymbol{\xi} - \boldsymbol{u}|^2 \frac{\partial f}{\partial \xi_j} \, \mathrm{d}\boldsymbol{\xi} = -2 \int_{\mathbb{R}^3} (\xi_j - u_j) f \, \mathrm{d}\boldsymbol{\xi} = 0. \tag{3.12}$$

Thus, the final form of equations for $|\alpha| \geqslant 2$ reads

$$\frac{\partial f_\alpha}{\partial t} - \frac{1}{f_0} \sum_{d=1}^{3} \sum_{j=1}^{3} \frac{\partial p_{jd}}{\partial x_j} f_{\alpha - e_d} - \frac{1}{3f_0} \sum_{j=1}^{3} \left(\frac{\partial q_j}{\partial x_j} + \sum_{d=1}^{3} p_{jd} \frac{\partial u_d}{\partial x_j} \right) \sum_{d=1}^{3} f_{\alpha - 2e_d}$$

$$+ \sum_{j,d=1}^{3} \left[\frac{\partial u_d}{\partial x_j} \left(\theta f_{\alpha - e_d - e_j} + (\alpha_j + 1) f_{\alpha - e_d + e_j} \right) + \frac{1}{2} \frac{\partial \theta}{\partial x_j} \left(\theta f_{\alpha - 2e_d - e_j} + (\alpha_j + 1) f_{\alpha - 2e_d + e_j} \right) \right]$$

$$+ \sum_{j=1}^{3} \left(\theta \frac{\partial f_{\alpha - e_j}}{\partial x_j} + u_j \frac{\partial f_\alpha}{\partial x_j} + (\alpha_j + 1) \frac{\partial f_{\alpha + e_j}}{\partial x_j} \right) = \frac{1}{\tau} \left(\frac{1 - \mathrm{Pr}}{5} \sum_{i,j=1}^{3} \delta_{ij}(\alpha) q_i - \delta(\alpha) f_\alpha \right). \tag{3.13}$$

In order to get a closed system, we collect (2.11), (3.10), (3.11) and (3.13) with $2 \leqslant |\alpha| \leqslant M$ together. Then the governing system for the NRxx method with Shakhov model and force terms is formed.

Remark 1. In the Shakhov model, the equation (2.11), the prediction of f_α with $|\alpha| = M+1$ derived for the BGK model, is still available. In [5], (2.11) is deduced in the following two steps:

1. Determine the orders of magnitude for all f_α using Maxwellian iteration.

2. For $|\alpha| = M + 1$, remove all the high order terms in the equations containing only $-f_\alpha/\tau$ in their right hand sides.

The Maxwellian iteration can also be applied to (3.13), and after the first iteration step, we immediately get

$$f_\alpha = O(\tau), \qquad |\alpha| = 2, \quad \text{or} \quad \alpha = e_i + 2e_j, \quad i, j = 1, 2, 3, \tag{3.14}$$

and other moments with $|\alpha| \geqslant 2$ remain to be zero. This result is the same as that we have derived in the BGK model. We note that for $|\alpha| > 3$ and $\alpha = (1, 1, 1)$, (3.13) is just the corresponding equation for the BGK model. Thus, in the view of order of magnitude, the subsequent iterations are identical to the BGK case. Moreover, when $M \geqslant 3$, which we have assumed in the last section, step 2 is also identical for both models. Hence (2.11) still applies for the Shakhov model.

3.2 The numerical approach

The acceleration $\boldsymbol{F}$ only appears in (3.10) in the governing system, thus a splitting method can be applied as follows:

1. *Transportation:* solve the force-free Shakhov equation over a time step of length Δt.

2. *Acceleration:* solve $\partial_t \boldsymbol{u} = \boldsymbol{F}$ over a time step of length Δt.

In order to solve the force-free Shakhov equation, another splitting of the convection and collision part is needed. For the convection part, the method is identical to that used in the BGK model. We refer the readers to [4, 6] for details. For the collision part, since a new collision model is adopted, the procedure is slightly different.

Now we consider the pure collision model, where ρ, $\boldsymbol{u}$ and θ are not changed while time evolves. Therefore, the collision terms only exist in (3.13) with $|\alpha| \geqslant 2$. Two cases are considered below:

(1) $\alpha = e_i + 2e_j$, $i, j = 1, 2, 3$. In these cases, the pure collision equations are written as

$$
\begin{aligned}
\frac{\partial f_{e_i + 2e_j}}{\partial t} &= \frac{(1 - \mathrm{Pr})q_i - 5 f_{e_i + 2e_j}}{5\tau} \\
&= \frac{1}{\tau}\left[\frac{1 - \mathrm{Pr}}{5}\left(2 f_{3e_i} + \sum_{j=1}^{3} f_{e_i + 2e_j} \right) - f_{e_i + 2e_j} \right], \qquad i, j = 1, 2, 3.
\end{aligned}
\tag{3.15}
$$

In the general case, τ only depends on ρ and θ. Thus it is invariant in the collision-only system. This turns (3.15) into a linear *ordinary* differential system with 9 equations, which can be analytically integrated as

$$
f_{e_i + 2e_j}(t) = \frac{1}{5}q_i(t_0)\exp\left(-\frac{\mathrm{Pr}(t - t_0)}{\tau} \right) - \left(\frac{1}{5}q_i(t_0) - f_{e_i + 2e_j}(t_0) \right)\exp\left(-\frac{t - t_0}{\tau} \right), \tag{3.16}
$$

where t_0 denotes the initial time.

(2) Other cases. For other α's, the collision-only equation is the same as the BGK model:

$$
\frac{\partial f_\alpha}{\partial t} = -\frac{1}{\tau}f_\alpha. \tag{3.17}
$$

The solution is

$$
f_\alpha(t) = f_\alpha(t_0)\exp\left(-\frac{t - t_0}{\tau} \right). \tag{3.18}
$$

When (3.16) and (3.18) are used in the numerical scheme, we replace t and t_0 with t_{n+1} and t_n respectively. Note that when τ is independent of $\boldsymbol{u}$, the acceleration and collision do not coupled with each other, thus the splitting is applied only once rather than twice. This makes it more efficient when the Strang splitting is employed.

4 Boundary conditions

In the moment methods, the boundary condition is always a complicated issue when simulating microflows. As discussed in [7, 20, 26, 28, 11] and the references therein, delicate derivations and careful numerical techniques are needed for a solid wall. In this section, a numerical way for dealing with boundary conditions in the NRxx method is introduced, which appears to be uniform for all orders of moment systems.

4.1 The kinetic boundary condition

In the kinetic theory, the most extensively used boundary condition is the one proposed by Maxwell in [15]. According to the common hyperbolic theory, for (2.3), the boundary condition is only needed when $\boldsymbol{\xi} \cdot \boldsymbol{n} < 0$, where $\boldsymbol{n}$ is the outer normal vector of the boundary. For a point $\boldsymbol{x}$ on the wall, supposing the velocity and temperature of the wall to be $\boldsymbol{u}^W(t, \boldsymbol{x})$ and $\theta^W(t, \boldsymbol{x})$ at time t, Maxwell proposed the following boundary condition:

$$f(t, \boldsymbol{x}, \boldsymbol{\xi}) = \begin{cases} \chi f_M^W(t, \boldsymbol{x}, \boldsymbol{\xi}) + (1 - \chi) f(t, \boldsymbol{x}, \boldsymbol{\xi}^*), & \boldsymbol{C}^W \cdot \boldsymbol{n} < 0, \\ f(t, \boldsymbol{x}, \boldsymbol{\xi}), & \boldsymbol{C}^W \cdot \boldsymbol{n} \geqslant 0, \end{cases} \tag{4.1}$$

where $\chi \in [0, 1]$ is a parameter for different gases and walls, and

$$\boldsymbol{\xi}^* = \boldsymbol{\xi} - 2(\boldsymbol{C}^W \cdot \boldsymbol{n})\boldsymbol{n}, \quad \boldsymbol{C}^W = \boldsymbol{\xi} - \boldsymbol{u}^W(t, \boldsymbol{x}), \tag{4.2}$$

$$f_M^W(t, \boldsymbol{x}, \boldsymbol{\xi}) = \frac{\rho^W(t, \boldsymbol{x})}{(2\pi\theta^W(t, \boldsymbol{x}))^{3/2}} \exp\left(-\frac{|\boldsymbol{\xi} - \boldsymbol{u}^W(t, \boldsymbol{x})|^2}{2\theta^W(t, \boldsymbol{x})}\right). \tag{4.3}$$

The functions $\boldsymbol{u}^W(t, \boldsymbol{x})$ and $\theta^W(t, \boldsymbol{x})$ are prescribed and stand for the wall velocity and temperature at time t and position $\boldsymbol{x}$, and $\rho^W(t, \boldsymbol{x})$ ensures the conservation of the mass at the wall, that is,

$$\int_{\mathbb{R}^3} (\boldsymbol{C}^W \cdot \boldsymbol{n}) f(t, \boldsymbol{x}, \boldsymbol{\xi}) \, \mathrm{d}\boldsymbol{\xi}$$
$$= \chi \left(\int_{\boldsymbol{C}^W \cdot \boldsymbol{n} < 0} (\boldsymbol{C}^W \cdot \boldsymbol{n}) f_M^W(t, \boldsymbol{x}, \boldsymbol{\xi}) \, \mathrm{d}\boldsymbol{\xi} + \int_{\boldsymbol{C}^W \cdot \boldsymbol{n} \geqslant 0} (\boldsymbol{C}^W \cdot \boldsymbol{n}) f(t, \boldsymbol{x}, \boldsymbol{\xi}) \, \mathrm{d}\boldsymbol{\xi} \right) = 0. \tag{4.4}$$

For this boundary condition, the normal velocity of gas on the boundary is the same as the normal velocity of the wall. However, in the case of shear flow, velocity slip and temperature jump will appear on the boundary.

4.2 The boundary conditions for the NRxx method

The boundary condition can be derived by taking moments on both sides on (4.1). Before that, we define

$$C_{\theta, \alpha} = \frac{(2\pi)^{3/2} \theta^{|\alpha|+3}}{\alpha_1! \alpha_2! \alpha_3!}, \qquad \forall \theta > 0, \quad \alpha \in \mathbb{N}^3. \tag{4.5}$$

This definition leads to

$$g_\alpha = C_{\theta, \alpha} \int_{\mathbb{R}^3} g(\boldsymbol{\xi}) \mathcal{H}_{\theta, \alpha}(\boldsymbol{v}) \exp(|\boldsymbol{v}|^2/2) \, \mathrm{d}\boldsymbol{v}, \tag{4.6}$$

where $\boldsymbol{v} = (\boldsymbol{\xi} - \boldsymbol{u})/\sqrt{\theta}$ and $g(\boldsymbol{\xi})$ is a distribution function expanded into Hermite series as $g(\boldsymbol{\xi}) = \sum_{\alpha \in \mathbb{N}^3} g_\alpha \mathcal{H}_{\theta, \alpha}(\boldsymbol{v})$. In order to simplify the calculation, we suppose $\boldsymbol{n} = (0, 1, 0)^T$. Thus, taking moments for (4.1) requires half-space integration

$$C_{\theta, \alpha} \int_{\xi_2 \geqslant u_2^W} g(\boldsymbol{\xi}) \mathcal{H}_{\theta, \alpha}(\boldsymbol{v}) \exp(|\boldsymbol{v}|^2/2) \, \mathrm{d}\boldsymbol{v}. \tag{4.7}$$

Suppose an M-th order system is used in the NRxx method; that is, an $(M+1)$-st order approximation of the distribution can be obtained through (2.11). This approximation is

directly used in (4.7) so that the integral can be actually worked out. Concretely speaking, (4.7) is approximated as

$$\sum_{|\beta|\leqslant M+1} g_\beta C_{\theta,\alpha} \int_{\xi_2 \geqslant u_2^W} \mathcal{H}_{\theta,\alpha}(\boldsymbol{v})\mathcal{H}_{\theta,\beta}(\boldsymbol{v})\exp(|\boldsymbol{v}|^2/2)\,\mathrm{d}\boldsymbol{v}. \tag{4.8}$$

Since $u_2 = u_2^W$ on the boundary, the region of integration can be written as $\{v_2 \geqslant 0\}$. Thus, we only need to calculate

$$I_{\alpha,\beta}(\theta) = C_{\theta,\alpha} \int_{v_2 \geqslant 0} \mathcal{H}_{\theta,\alpha}(\boldsymbol{v})\mathcal{H}_{\theta,\beta}(\boldsymbol{v})\exp(|\boldsymbol{v}|^2/2)\,\mathrm{d}\boldsymbol{v}. \tag{4.9}$$

The details can be found in Appendix B, and the result is

$$I_{\alpha,\beta}(\theta) = S(\alpha_2, \beta_2)\theta^{\frac{\alpha_2 - \beta_2}{2}} \cdot \delta_{\alpha_1\beta_1}\delta_{\alpha_3\beta_3} \tag{4.10}$$

and

$$S(m,n) = \begin{cases} 1/2, & m = n = 0, \\ K(1, n-1), & m = 0 \text{ and } n \neq 0, \\ K(m,0), & m \neq 0 \text{ and } n = 0, \\ K(m,n) + S(m-1, n-1) \cdot n/m, & \text{otherwise,} \end{cases} \tag{4.11}$$

where

$$K(m,n) = \frac{(2\pi)^{-1/2}}{m!} He_{m-1}(0) He_n(0). \tag{4.12}$$

The above deduction leads to the following proposition:

Proposition 1. *Suppose $g(\boldsymbol{v})$ is a function defined on $\mathbb{R}^3$ which can be denoted by a finite expansion of Hermite basis functions*

$$g(\boldsymbol{v}) = \sum_{|\alpha|\leqslant M+1} g_\alpha \mathcal{H}_{\theta,\alpha}(\boldsymbol{v}). \tag{4.13}$$

for some $\theta > 0$. Let $\tilde{g}(\boldsymbol{v})$ be a half-space cut-off of $g(\boldsymbol{v})$ as

$$\tilde{g}(\boldsymbol{v}) = \begin{cases} g(\boldsymbol{v}), & v_2 \geqslant 0, \\ 0, & v_2 < 0. \end{cases} \tag{4.14}$$

Then $\tilde{g}$ can also be expanded into Hermite series as

$$\tilde{g}(\boldsymbol{v}) = \sum_{\alpha\in\mathbb{N}^3} \sum_{|\beta|\leqslant M+1} g_\beta I_{\alpha,\beta}(\theta)\mathcal{H}_{\theta,\alpha}(\boldsymbol{v}), \tag{4.15}$$

where $I_{\alpha,\beta}(\theta)$ is defined in (4.10)—(4.12).

Proof. It is already known in [4] that $\{\mathcal{H}_{\theta,\alpha}(\boldsymbol{v})\}_{\alpha\in\mathbb{N}^3}$ is an orthogonal basis of the weighted L^2 space $L^2(\mathbb{R}^3; \exp(|\boldsymbol{v}|^2/2)\,\mathrm{d}\boldsymbol{v})$. Since

$$\begin{aligned} \int_{\mathbb{R}^3} |\tilde{g}(\boldsymbol{v})|^2 \exp(|\boldsymbol{v}|^2/2)\,\mathrm{d}\boldsymbol{v} &= \int_{v_2\geqslant 0} |g(\boldsymbol{v})|^2 \exp(|\boldsymbol{v}|^2/2)\,\mathrm{d}\boldsymbol{v} \\ &\leqslant \int_{\mathbb{R}^3} |g(\boldsymbol{v})|^2 \exp(|\boldsymbol{v}|^2/2)\,\mathrm{d}\boldsymbol{v} = \sum_{|\alpha|\leqslant M+1} C_{\theta,\alpha}^{-1}|g_\alpha|^2 < +\infty, \end{aligned} \tag{4.16}$$

$\tilde{g}(\boldsymbol{v})$ also lies in $L^2(\mathbb{R}^3; \exp(|\boldsymbol{v}|^2/2)\,\mathrm{d}\boldsymbol{v})$. Thus the validity of (4.15) can be naturally obtained. $\qquad\square$

The following proposition depicts the sparsity of $I_{\alpha,\beta}$.

Proposition 2. *If $I_{\alpha,\beta}(\theta)$ is nonzero, then (1) $\alpha_1 = \beta_1$; (2) $\alpha_3 = \beta_3$; (3) $\alpha_2 - \beta_2$ is zero or odd. When $\alpha = \beta$, $I_{\alpha,\beta}(\theta)$ is equal to $1/2$.*

Proof. If $I_{\alpha,\beta}(\theta)$ is nonzero, (4.10) directly gives $\alpha_1 = \beta_1$ and $\alpha_3 = \beta_3$. If $\alpha_2 - \beta_2$ is a nonzero even integer, $K(\alpha_2, \beta_2)$ is zero since $He_n(0)$ is zero when n is odd. In order to prove $I_{\alpha,\beta}(\theta) = 0$ in this case, according to (4.10), we only need to prove $S(\alpha_2, \beta_2) = 0$. This can be done by induction:

(1) If $\alpha_2 = 0$ or $\beta_2 = 0$, α_2 and β_2 must be both even but one of them must be positive. Equation (4.11) shows $S(\alpha_2, \beta_2) = 0$ directly.

(2) Suppose $S(\alpha_2 - 1, \beta_2 - 1) = 0$. Then, according to the last case in (4.11), $S(\alpha_2, \beta_2)$ is also zero.

Finally, when $\alpha = \beta$, (4.10) gives $I_{\alpha,\beta}(\theta) = S(\alpha_2, \beta_2)$. The subsequent proof can also be done by induction, since $S(0,0) = 1/2$ and $K(n,n) = 0$ for $n > 0$. $\qquad\square$

According to Proposition 2, we find that only $(\lceil \alpha_2/2 \rceil + 1)$ terms are nonzero in the summation (4.8). This greatly reduces the computational cost.

Now let us return to the boundary conditions. According to Grad's theory [7, 9], in order to ensure the continuity of boundary conditions when $\chi \to 0$, only a subset of moments $\{f_\alpha \mid |\alpha| \leqslant M + 1$ and α_2 is odd$\}$ should be used to formulate boundary conditions. This will be completed in the following three subsections. Later in this section, for conciseness, the variables t and $\boldsymbol{x}$ are omitted in our statement if not specified, and all spatially dependent functions are considered to be on the boundary.

4.2.1 Determination of ρ^W

For simplicity, we factorize the right hand side of (4.1) into three parts and consider each part independently. Define

$$p(\boldsymbol{\xi}) = \begin{cases} f_M^W(\boldsymbol{\xi}), & \xi_2 < u_2^W, \\ 0, & \xi_2 \geqslant u_2^W, \end{cases} \quad q(\boldsymbol{\xi}) = \begin{cases} f(\boldsymbol{\xi}), & \xi_2 \geqslant u_2^W, \\ 0, & \xi_2 < u_2^W, \end{cases} \quad r(\boldsymbol{\xi}) = q(\boldsymbol{\xi}) + q(\boldsymbol{\xi}^*).$$
(4.17)

Then (4.1) can be rewritten as

$$f(\boldsymbol{\xi}) = \chi p(\boldsymbol{\xi}) + \chi q(\boldsymbol{\xi}) + (1 - \chi) r(\boldsymbol{\xi}).$$
(4.18)

Suppose the Hermite expansion of f is

$$f(\boldsymbol{\xi}) = \sum_{|\alpha| \leqslant M+1} f_\alpha \mathcal{H}_{\theta,\alpha} \left(\frac{\boldsymbol{\xi} - \boldsymbol{u}}{\sqrt{\theta}} \right).$$
(4.19)

Then $q(\boldsymbol{\xi})$ can also be expanded into Hermite series according to Proposition 1 and 2 as

$$q(\boldsymbol{\xi}) = \sum_{\alpha \in \mathbb{N}^3} q_\alpha \mathcal{H}_{\theta,\alpha} \left(\frac{\boldsymbol{\xi} - \boldsymbol{u}}{\sqrt{\theta}} \right).$$
(4.20)

Substituting (4.3) and (4.20) into (4.4), ρ^W can be worked out as

$$\rho^W = \sqrt{\frac{2\pi}{\theta^W}} q_{e_2} = \sqrt{\frac{2\pi}{\theta^W}} \sum_{k=0}^{\lceil M/2 \rceil} S(1, 2k) \theta^{1/2-k} f_{2ke_2},$$
(4.21)

where the expression of q_{e_2} is derived from (4.10), (4.15) and Proposition 2.

11

4.2.2 The moments of p and r

Now the moments for $q(\boldsymbol{\xi})$ have been calculated in (4.20), we still need to get Hermite expansions of $p(\boldsymbol{\xi})$ and $r(\boldsymbol{\xi})$. We suppose that $p(\boldsymbol{\xi})$ can be expanded under the basis $\left\{\mathcal{H}_{\theta,\alpha}\big((\boldsymbol{\xi}-\boldsymbol{u})/\sqrt{\theta}\big)\right\}_{\alpha\in\mathbb{N}^3}$ as

$$p(\boldsymbol{\xi}) = \sum_{\alpha\in\mathbb{N}^3} p_\alpha \mathcal{H}_{\theta,\alpha}\left(\frac{\boldsymbol{\xi}-\boldsymbol{u}}{\sqrt{\theta}}\right). \tag{4.22}$$

Then, according to (4.3), the coefficients can be formulated by

$$p_\alpha = C_{\theta,\alpha} \int_{v_2<0} \frac{\rho^W}{(2\pi\theta^W)^{3/2}} \exp\left(-\frac{|\boldsymbol{\xi}-\boldsymbol{u}^W|^2}{2\theta^W}\right) \mathcal{H}_{\theta,\alpha}(\boldsymbol{v}) \exp\left(\frac{|\boldsymbol{v}|^2}{2}\right) \mathrm{d}\boldsymbol{v}, \tag{4.23}$$

where $\boldsymbol{\xi} = \sqrt{\theta}\boldsymbol{v} + \boldsymbol{u}$. Define

$$J_s(x) = \frac{1}{s!}\theta^{\frac{s+1}{2}} \int_{-\infty}^{+\infty} \frac{1}{\sqrt{2\pi\theta^W}} \exp\left(-\frac{|\sqrt{\theta}y-x|^2}{2\theta^W}\right) He_s(y)\,\mathrm{d}y, \tag{4.24}$$

$$\tilde{J}_s(x) = \frac{1}{s!}\theta^{\frac{s+1}{2}} \int_{-\infty}^{0} \frac{1}{\sqrt{2\pi\theta^W}} \exp\left(-\frac{|\sqrt{\theta}y-x|^2}{2\theta^W}\right) He_s(y)\,\mathrm{d}y. \tag{4.25}$$

Then p_α can be expressed by

$$p_\alpha = \rho^W J_{\alpha_1}(u_1^W - u_1)\tilde{J}_{\alpha_2}(u_2^W - u_2) J_{\alpha_3}(u_3^W - u_3). \tag{4.26}$$

$J_s(x)$ and $\tilde{J}_s(x)$ can be calculated recursively as

$$J_s(x) = \frac{1}{s}\left[(\theta^W - \theta)J_{s-2}(x) + xJ_{s-1}(x)\right], \quad s \geqslant 1; \tag{4.27}$$

$$\tilde{J}_s(x) = \frac{1}{s}\left[(\theta^W - \theta)\tilde{J}_{s-2}(x) + x\tilde{J}_{s-1}(x)\right] - H_s(x), \quad s \geqslant 1; \tag{4.28}$$

$$H_s(x) = -\frac{s-2}{s(s-1)}\theta H_{s-2}(x), \quad s \geqslant 2. \tag{4.29}$$

The starting values are

$$J_{-1}(x) = 0, \qquad J_0(x) = 1, \tag{4.30}$$

$$\tilde{J}_{-1}(x) = 0, \qquad \tilde{J}_0(x) = \frac{1}{2}\mathrm{erfc}\left(\frac{x}{\sqrt{2\theta^W}}\right), \tag{4.31}$$

$$H_0(x) = 0, \qquad H_1(x) = \sqrt{\frac{\theta^W}{2\pi}}\exp\left(-\frac{x^2}{2\theta^W}\right), \tag{4.32}$$

The detailed derivation of (4.27)-(4.32) can be found in the Appendix C. Noting that $u_2 = u_2^W$, (4.26) can be further simplified as

$$p_\alpha = \rho^W J_{\alpha_1}(u_1^W - u_1)\hat{J}_{\alpha_2} J_{\alpha_3}(u_3^W - u_3), \tag{4.33}$$

where

$$\hat{J}_s = \frac{1}{s}(\theta^W - \theta)\hat{J}_{s-2} - \hat{H}_s, \quad s \geqslant 1, \qquad \hat{H}_s = -\frac{s-2}{s(s-1)}\theta\hat{H}_{s-2}, \quad s \geqslant 2,$$

$$\hat{J}_{-1} = \hat{H}_0 = 0, \quad \hat{J}_0 = 1/2, \quad \hat{H}_1 = \sqrt{\frac{\theta^W}{2\pi}}. \tag{4.34}$$

12

Here we emphasize that due to equation (4.21), all p_α's are only related with $\{f_{2ke_2}\}_{0 \leqslant k \leqslant \lceil M/2 \rceil}$ besides $\boldsymbol{u}$, $\boldsymbol{u}^W$, θ and θ^W.

Now we turn to the moments of $r(\boldsymbol{\xi})$. Note that only the moments with odd α_2 are needed. However, $r(\boldsymbol{\xi})$ is an even function with respect to C_2^W, which causes all its moments with odd α_2 vanished. This indicates that $r(\boldsymbol{\xi})$ can be simply neglected when discussing the boundary conditions.

4.2.3 Construction of boundary conditions

Now we take moments with odd α_2 on both sides of (4.18). Making use of Proposition 2, we have

$$f_\alpha = \chi p_\alpha + \chi q_\alpha = \chi p_\alpha + \frac{1}{2}\chi f_\alpha + \chi \sum_{k=0}^{K_2(\alpha)} S(\alpha_2, 2k)\theta^{\alpha_2/2-k} f_{\alpha+(2k-\alpha_2)e_2}, \tag{4.35}$$

where $K_2(\alpha) = \lceil (M - \alpha_1 - \alpha_3)/2 \rceil$. A simple rearrangement gives

$$f_\alpha = \frac{2\chi}{2-\chi} \left[p_\alpha + \sum_{k=0}^{K_2(\alpha)} S(\alpha_2, 2k)\theta^{\alpha_2/2-k} f_{\alpha+(2k-\alpha_2)e_2} \right]. \tag{4.36}$$

Equations (4.36) with $|\alpha| \leqslant M+1$ and odd α_2, together with $u_2 = u_2^W$ form the boundary conditions of the dynamic moment equations. Recalling

$$p_\alpha = p_\alpha(\boldsymbol{u}, \boldsymbol{u}^W, \theta, \theta^W, f_0, f_{2e_2}, \cdots, f_{2\lceil M/2 \rceil e_2}), \tag{4.37}$$

one can find that the terms which appear on the left hand side of (4.36) never appear on its right hand side. Thus, if an arbitrary distribution function denoted as (4.19) is given, we can define a functional F^b which maps (4.19) to another distribution $f^b(\boldsymbol{\xi})$:

$$f^b(\boldsymbol{\xi}) = \sum_{|\alpha| \leqslant M+1} f_\alpha^b \mathcal{H}_{\theta^b, \alpha}\left(\frac{\boldsymbol{\xi} - \boldsymbol{u}^b}{\sqrt{\theta^b}}\right), \tag{4.38}$$

where $\boldsymbol{u}^b = (u_1, u_2^W, u_3)$, $\theta^b = \theta$, and

$$f_\alpha^b = \begin{cases} f_\alpha, & \text{if } \alpha_2 \text{ is even,} \\ \text{the right hand side of (4.36)}, & \text{if } \alpha_2 \text{ is odd.} \end{cases} \tag{4.39}$$

Thus f_α^b satisfies the boundary condition. The mapping F^b will be used in the numerical implementation of boundary conditions.

At the end of this section, we prove that $\boldsymbol{u}^b$ and θ^b are the corresponding velocity and temperature of the distribution function $f^b(\boldsymbol{\xi})$. This is equivalent to the following proposition:

Proposition 3. *If a distribution $f(\boldsymbol{\xi})$ with expression (4.19) satisfies*

$$f_{e_1} = f_{e_2} = f_{e_3} = \sum_{d=1}^{3} f_{2e_d} = 0, \tag{4.40}$$

then $f^b = F^b(f)$ with expression (4.38) also satisfies

$$f_{e_1}^b = f_{e_2}^b = f_{e_3}^b = \sum_{d=1}^{3} f_{2e_d}^b = 0. \tag{4.41}$$

13

Proof. Equation (4.39) gives

$$f^b_{e_1} = f_{e_1}, \qquad f^b_{e_3} = f_{e_3}, \qquad f^b_{2e_d} = f_{2e_d}, \quad d = 1, 2, 3. \tag{4.42}$$

Thus it only remains to prove $f^b_{e_2} = 0$. According to (4.30), (4.33) and (4.34), p_{e_2} can actually be expressed by

$$p_{e_2} = \rho^W J_0(u^W_1 - u_1)\hat{J}_1 J_0(u^W_3 - u_3) = \rho^W[(\theta^W - \theta)\hat{J}_{-1} - \hat{H}_1] = -\rho^W\sqrt{\frac{\theta^W}{2\pi}}. \tag{4.43}$$

Since $K_2(e_2) = \lceil M/2 \rceil$, the above equation together with (4.21) and (4.36) immediately gives $f^b_{e_2} = 0$. $\qquad\square$

4.3 Numerical implementation of boundary conditions

In a finite volume scheme, the boundary conditions is often applied by ghost cell techniques. Suppose the distribution function of the cell on the boundary is denoted as (4.19). The distribution function of the ghost cell can be constructed as follows:

1. Apply F^b on $f(\boldsymbol{\xi})$ and suppose the result is (4.38);
2. Construct the ghost cell distribution as

$$f^{\text{ghost}}(\boldsymbol{\xi}) = \sum_{|\alpha| \leqslant M+1} (2f^b_\alpha - f_\alpha)\mathcal{H}_{\theta,\alpha}\left(\frac{\boldsymbol{\xi} - (2\boldsymbol{u}^b - \boldsymbol{u})}{\sqrt{\theta}}\right). \tag{4.44}$$

Now we consider the time complexity of this operation. Suppose $N_M = (M+2)(M+3)(M+4)/6$ is the number of moments involved in the boundary condition. Obviously, (4.44) requires $O(N_M)$ operations. For the calculation of $F^b(f)$, we list the cost as follows:

1. Half-space cut-off of f (4.20): $O(MN_M)$ operations;
2. Calculation of ρ^W (4.21): $O(1)$ operations;
3. Calculation of p_α (4.33): $O(N_M)$ operations;
4. Evaluation of (4.39): $O(N_M)$ operations.

Thus, the total computational cost is $O(MN_M)$, while the time complexity is $O(N_M)$ if no boundary condition is considered. However, since this procedure only takes place on the boundary, it produces little increment of the computational time in real computation.

Remark 2. Proposition 3 indicates the conservation of mass on the boundary when using the HLL numerical flux as in [6]. One can find that when $u^W_2 = 0$, saying a special reference coordinate system is used, the minimum and maximum signal speeds in need of the HLL flux are opposite numbers. Together with $\rho^{\text{ghost}} = \rho$, $u^{\text{ghost}}_2 = -u_2$, the mass conservation of the HLL scheme follows naturally.

5 Numerical examples

In this section, three numerical examples are presented to validate our algorithm. In all these examples, a hard sphere gas is assumed, for which the relaxation time is defined as

$$\tau = \frac{5}{16}\sqrt{\frac{2\pi}{\theta}}\frac{Kn}{\rho} \tag{5.1}$$

following [3], where Kn is the Knudsen number. The CFL number is always 0.95. And for all the tests, the wall is set to be a fully diffusive one ($\chi = 1$) with $\theta^W = 1$. The POSIX multithreading technique is utilized in our simulation, and at most 8 CPU cores are used.

5.1 The beginning of a shock wave's formation

The first example is a simulation of the interaction of a coming flow with a diffusive wall. The computational domain is $[-5, 0]$ and the global Knudsen number Kn used in (5.1) is set to be 0.5. The left boundary is a free boundary, and the right is a stationary diffusive wall parallel to the xz-plane. The initial condition is given by

$$\rho_0(y) = 1.0, \quad \boldsymbol{u}_0(y) = (0, 0.5, 0)^T, \quad \theta_0(y) = 1.0, \qquad \forall y \in [-5, 0], \qquad (5.2)$$

and the gas is in equilibrium everywhere. A left-going shock wave will form after a sufficiently long time. Here we stop the computation at $t = 1.0$ in order to check the validity of the boundary condition. For a reference solution, we solve the Shakhov equation (2.3) directly using a Conservative Discrete Velocity Method (CDVM) introduced in [27]. For the computation of both NRxx method and CDVM, a uniform mesh with 500 grids are used to discretize the domain. For CDVM, the computational velocity domain is $[-10, 10] \times [-10, 10] \times [-10, 10]$ and discretized by $50 \times 100 \times 50$ grids.

Figure 1 and 2 are the results for CDVM and NRxx method for $M = 3$ to 12. Only the part $y \in [-3, 0]$ is shown since all variables for the remaining part are almost constant. Since a large Knudsen number is considered, predictions from lower order moment equations give very large deviations, so the necessity of high order moment theory is obvious. As the number of moments increases, all profiles get closer and closer to the results of CDVM. When M reaches 11, the density and temperature plots agree with the CDVM results very well, and the errors in σ_{22} and q_2 are much smaller than the low order cases, though it is still observable. It is reasonable that higher order moments converge more slowly than lower order moments, which is also observed in [11].

5.2 Planar Couette flow

The planar Couette flow is a classic benchmark test in the field of microflows. The moment method for this problem has been investigated in a lot of papers such as [25, 18, 26, 10, 28, 11]. Here we consider the symmetric Couette flow. The gas lies between two plates parallel to the xz-plane. Two plates move in the opposite direction with constant velocities within their own planes. A steady state can be obtained for a fully developed flow.

In this example, the computational domain is $[-0.5, 0.5]$. The velocities of the left and right plates are

$$\boldsymbol{u}_L^W = (-0.6296, 0, 0)^T, \quad \boldsymbol{u}_R^W = (0.6296, 0, 0)^T. \qquad (5.3)$$

The initial state is a global equilibrium with

$$\rho_0(y) = 1, \quad \boldsymbol{u}_0(y) = 0, \quad \theta_0(y) = 1, \qquad \forall y \in [-0.5, 0.5]. \qquad (5.4)$$

The steady state can be achieved if the computational time is sufficiently long. Also, both the NRxx method and CDVM are applied to this problem. Three different Knudsen numbers, $Kn = 0.1, 0.5, 1.0$, are investigated. For CDVM, the computational velocity domain is chosen as $[-10, 10] \times [-10, 10] \times [-10, 10]$, and $50 \times 50 \times 50$ grids are used. Here
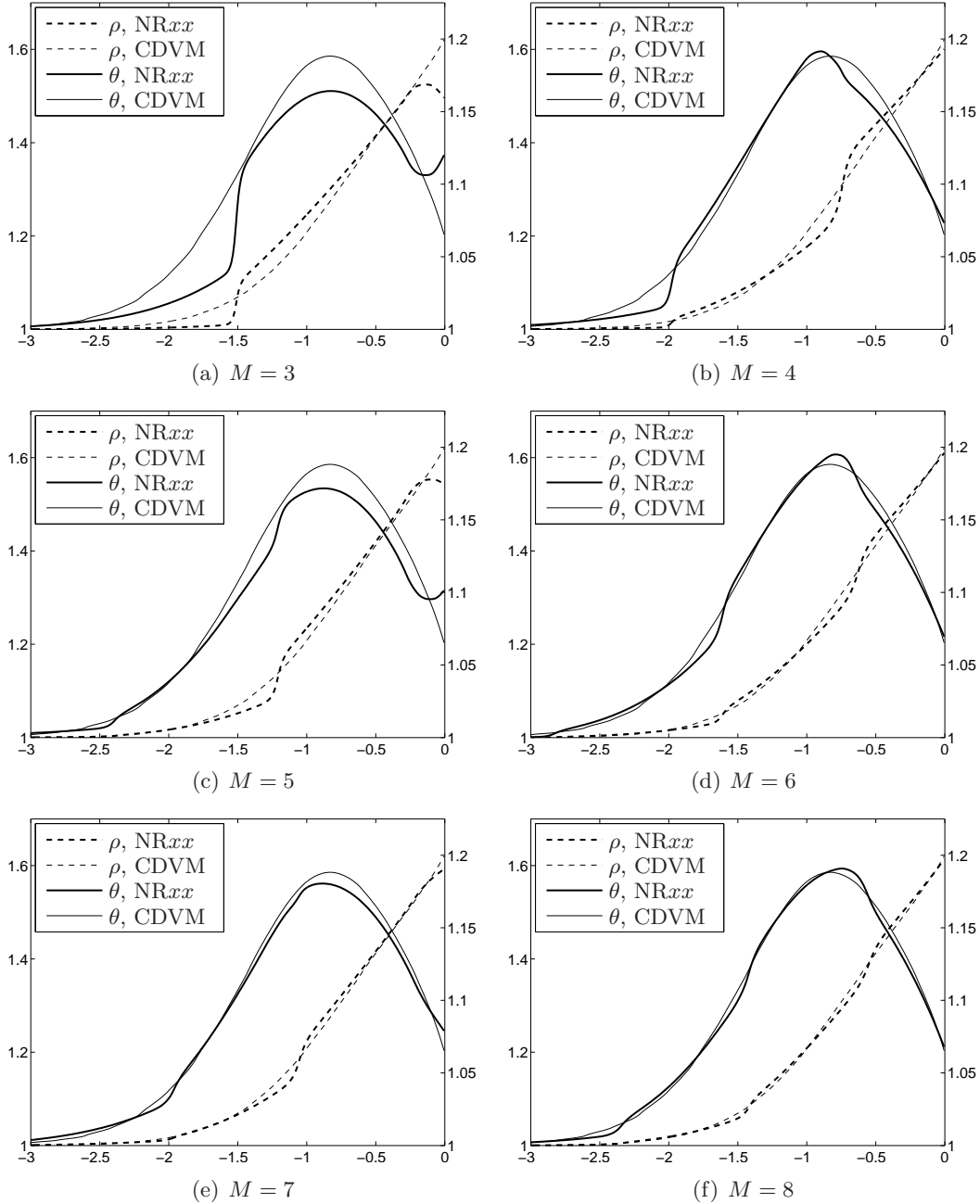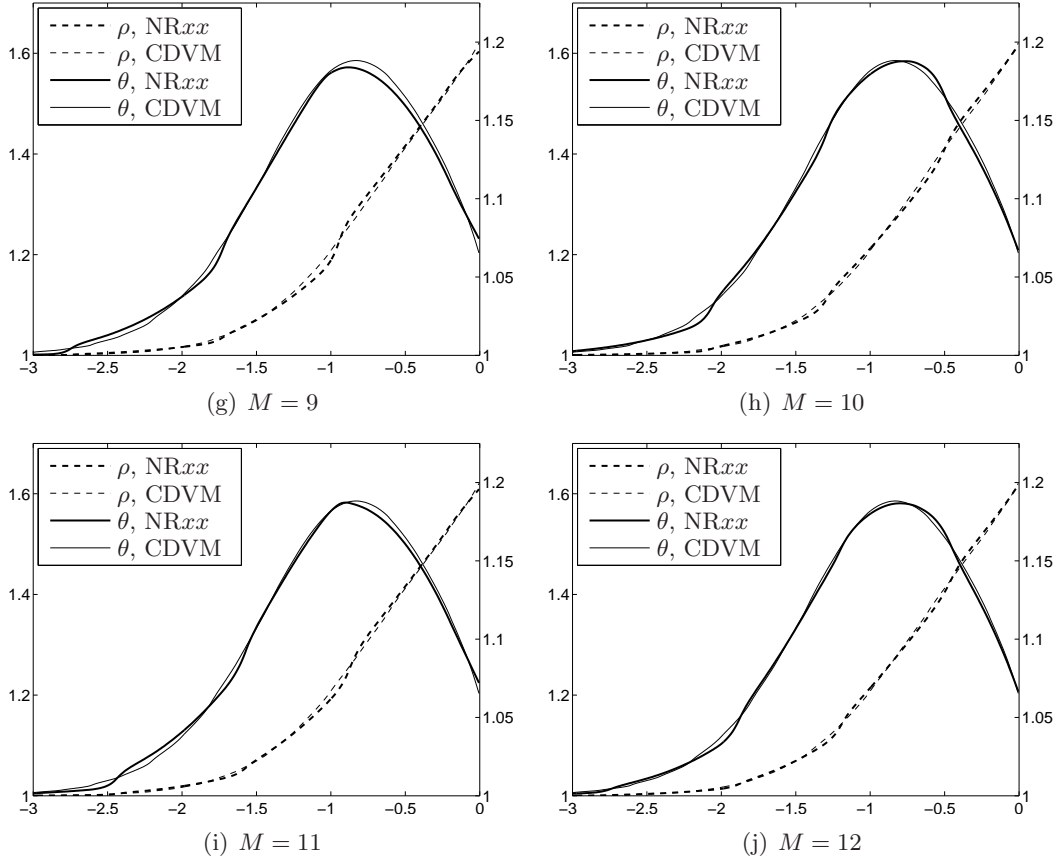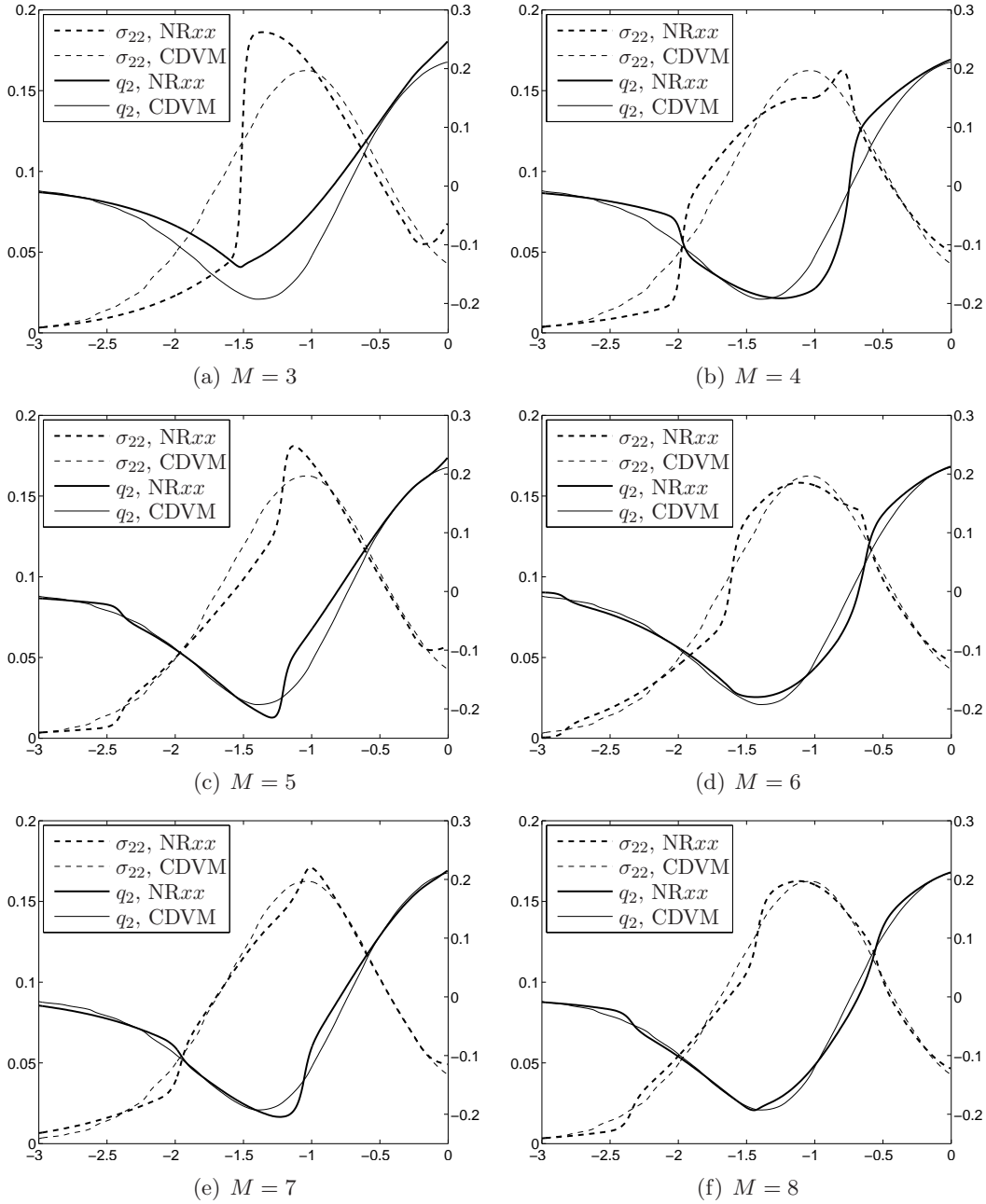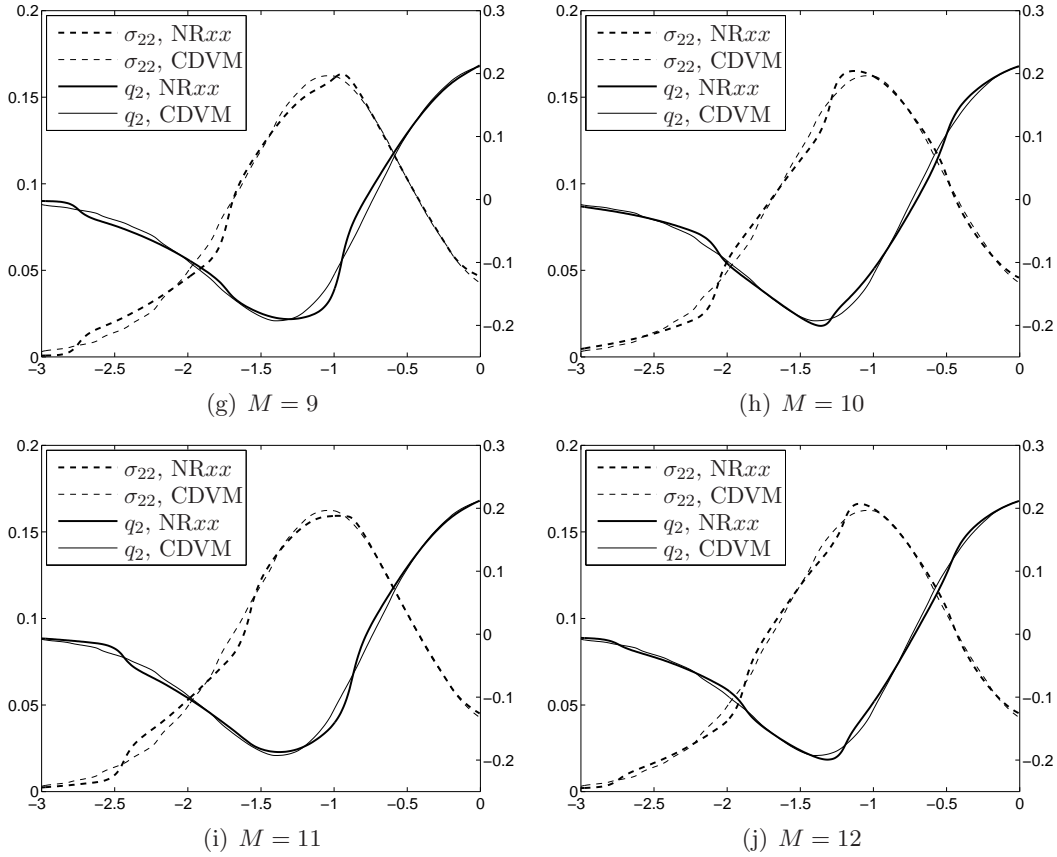
15

Figure 1: Density and temperature plots for the problem in section 5.1. The left axis is for the dashed lines, and the right axis is for the solid lines (to be continued).

we note that such discretization may not produce numerical results accurate enough as the reference solution, but the computation is already extremely slow.

Numerical results for $Kn = 0.1$ are shown in Figure 3 and 4. In this case, most lines agree with each other. The convergence in the number of moments can be observed, however, due to the numerical error from both NRxx method and CDVM, small deviations between the CDVM results and the possible limit of the NRxx method can be found. One can disclose that lower order NRxx results deviate from the CDVM results more

Figure 1: Density and temperature plots for the problem in section 5.1. The left axis is for the dashed lines, and the right axis is for the solid lines.

than higher order ones. This correctly reflects the behavior of NRxx method under low Knudsen numbers, as is also found by [4].

Now a larger Knudsen number $Kn = 0.5$ is considered, and the results are given in Figure 5 and 6. In this case, the results for odd and even orders evidently break into two groups, and they approach closer to the CDVM results separately. This can be also find in Figure 1 and 2. For ρ and θ, the even group gives better results, while for σ_{12} and σ_{22}, the odd group is more accurate. The reason remains to be further explored. The two subfigures in Figure 6 clearly exhibit the convergence. In [28, 11], it was discovered that the normal stress σ_{22} is difficult to match by R13 and R26 equations. Here one may find that when the number of moments is increasing, the quality of the approximation to this quantity is improved continuously. In case of $M = 9$, the profile agrees with the CDVM result quite well, and when $M = 10$, the relative difference is below 5%.

The severe case $Kn = 1.0$ is also studied. Similar results with the case $Kn = 0.5$ are obtained in Figure 7 and 8, while the magnitude of the difference is much larger. For σ_{22}, now the relative difference for $M = 9$ is about 10%. But the rate of convergence is still encouraging — compared with the result with $M = 4$, the error is halved.

17

Sfrag replacements
PSfrag replacements
Sfrag replacements
PSfrag replacements
Sfrag replacements
PSfrag replacements

Figure 2: Stress and heat flux plots for the problem in section 5.1. The left axis is for the dashed lines, and the right axis is for the solid lines (to be continued).

5.3 Force-driven Poiseuille flow

This is another example which is frequently used to verify the boundary conditions of moment methods [28, 11]. Similar with the Couette flow, the gas also lies between two parallel plates, but the plates are stationary and an external constant force parallel to the plates causes the flow to reach a non-stationary steady state. In our settings, the computational domain is again $[-0.5, 0.5]$, and the Knudsen number is set to be 0.1. The

Figure 2: Stress and heat flux plots for the problem in section 5.1. The left axis is for the dashed lines, and the right axis is for the solid lines.

force introduces an acceleration

$$\boldsymbol{F} = (0.2555, 0, 0)^T. \tag{5.5}$$

The initial condition is the same as the Couette flow. These settings are the non-dimensional form of the test in [32], where the DSMC result is carried out, and this example is also considered in [30, 11]. Since it is quite difficult for us to exert the force term in CDVM, we have to use the DSMC result in [32] for comparison in spite of the difference in the collision model.

The numerical results are presented in Figure 9 and 10. For all the profiles, the convergence in the number of moments is legible, while the NRxx results do not converge to the results of DSMC. This may due to the difference between the collision terms of Shakhov model and DSMC. Taking the temperature plot (Figure 9(c)) as an example, the result of $M = 3$ matches DSMC result best, since when $M = 3$, the collision term of Shakhov model is almost the same as that of DSMC. While when the number of moments increases, the collision term deviates away from DSMC's gradually. Here the accuracy of collision models is not the topic of this paper. Even though, two results are very close quantitatively, which indicates the correctness of the boundary conditions and the Prandtl number of the NRxx method.
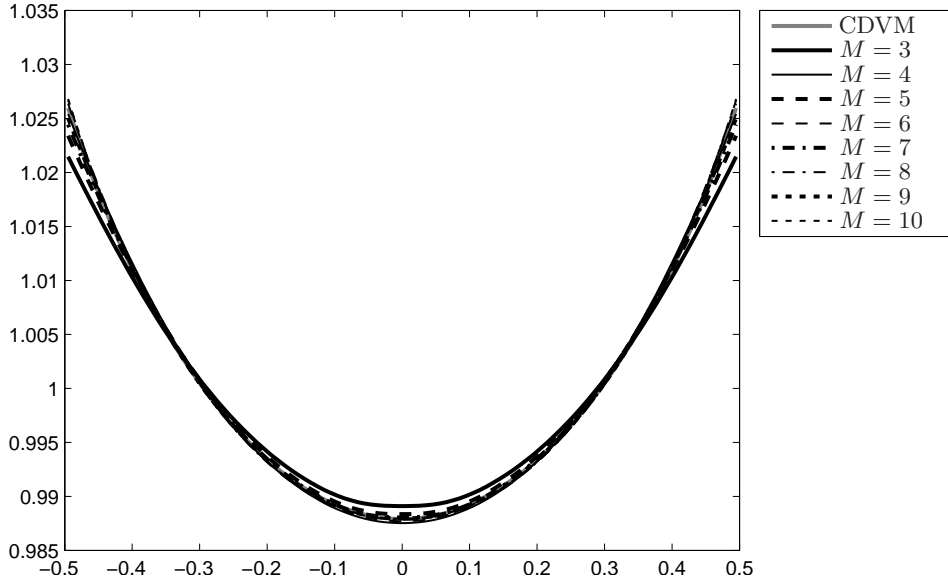
(a) Density, ρ
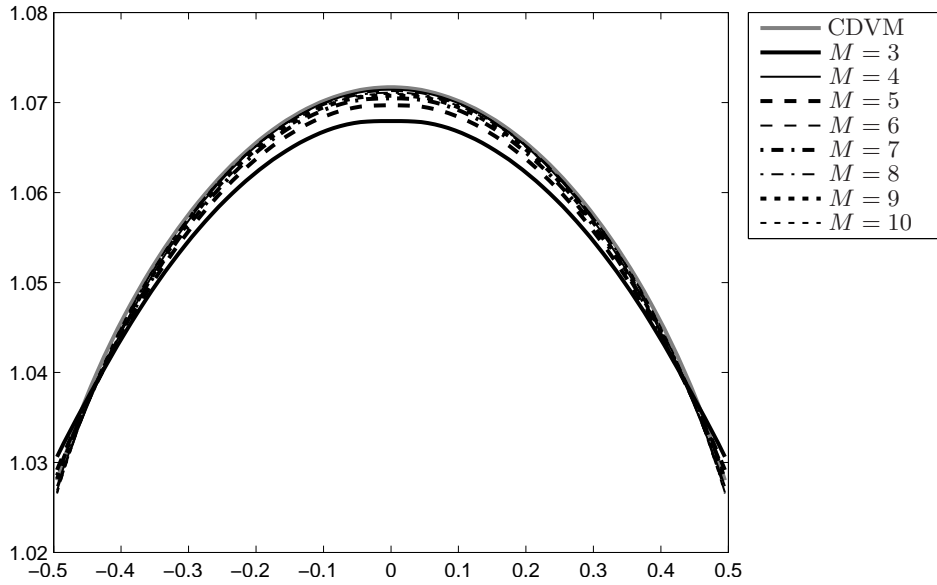
(b) Temperature, θ

Figure 3: Density and temperature plots for the planar Couette flow with $Kn = 0.1$ (to be continued)

6 Some discussions on the NRxx method

6.1 Order of accuracy

For the macroscopic equations, a basic quantity describing its ability is the *order of accuracy* with respect the Knudsen number. The definition of *order of accuracy* can be found in textbook [22]:

A set of equations is said to be accurate of order λ_0, when the pressure deviator
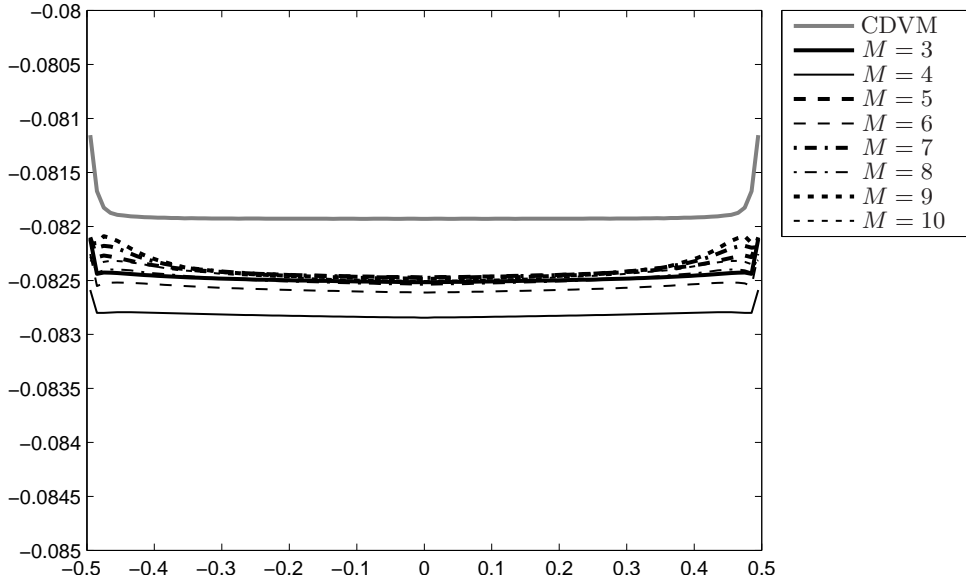
(a) Shear stress, σ_{12}
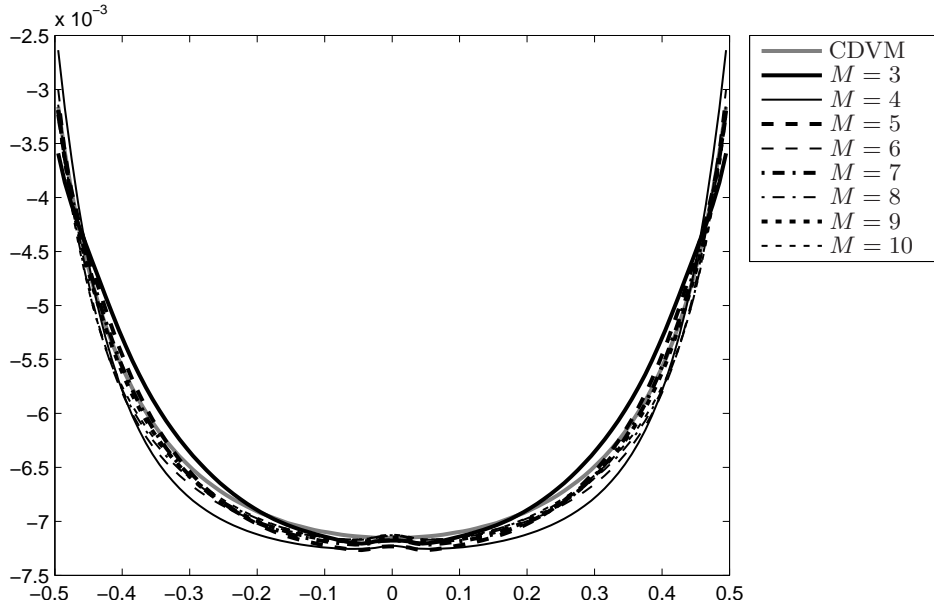
(b) Normal stress, σ_{22}

Figure 4: Shear and normal stress plots for the planar Couette flow with $Kn = 0.1$

> σ_{ij} and the heat flux q_i are known within the order $O(\varepsilon^{\lambda_0})$.

Here ε is a small parameter proportional to the relaxation time τ. As we have discussed in Remark 1, in the view of order of magnitude, the process of Maxwellian iteration for the Shakhov model is identical to the BGK model. Hence, for an arbitrary $M \geqslant 3$, the leading order term of f_α with $|\alpha| = M + 1$ is known from the corresponding moment equations (see [5] for details). And it has been deduced in [5] that $f_\alpha \sim O(\tau^{\lceil |\alpha|/3 \rceil})$ for all $|\alpha| \geqslant 4$. Thus, from the analytical form of the moment equations (3.13), we immediately have that f_α with $|\alpha| = M$ is known up to $(\lceil (M + 1)/3 \rceil + 1)$-th order. Subsequently, f_α

PSfrag replacements

DSMC

(a) Density, ρ

PSfrag replacements

DSMC
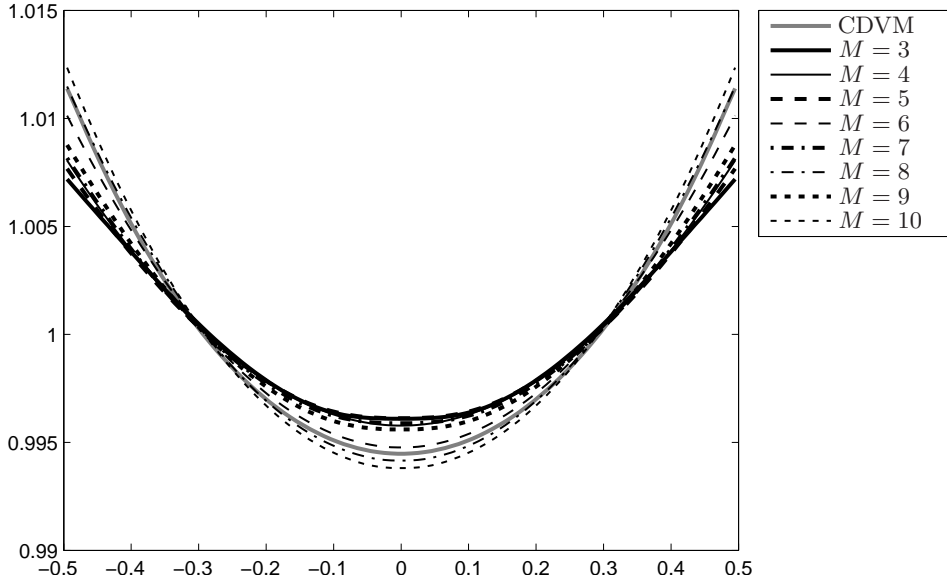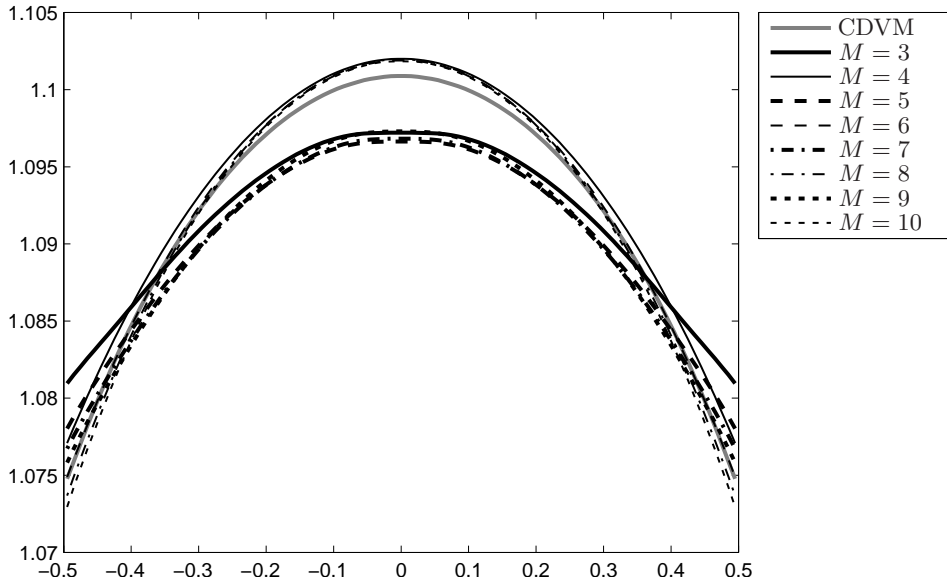
(b) Temperature, θ

Figure 5: Density and temperature plots for the planar Couette flow with $Kn = 0.5$

with $|\alpha| = M - 1$ is know up to $(\lceil (M + 1)/3 \rceil + 2)$-th order, and this can be done until $|\alpha| = 2$. The general result is

Proposition 4. *For the moment equations described in Section 3.1, f_α has $(\lceil 4(M + 1)/3 \rceil - |\alpha|)$-th order accuracy if $2 \leqslant |\alpha| \leqslant M$.*

Now, using (2.9) and the definition of order of accuracy, we conclude that the NRxx equations have the order of accuracy $\lceil (4M - 5)/3 \rceil$.

For boundary value problems, such discussion is only valid in the bulk. In the Knudsen layer, which is known to be of width $O(Kn)$, we need to use $X = x/Kn$ as the spatial
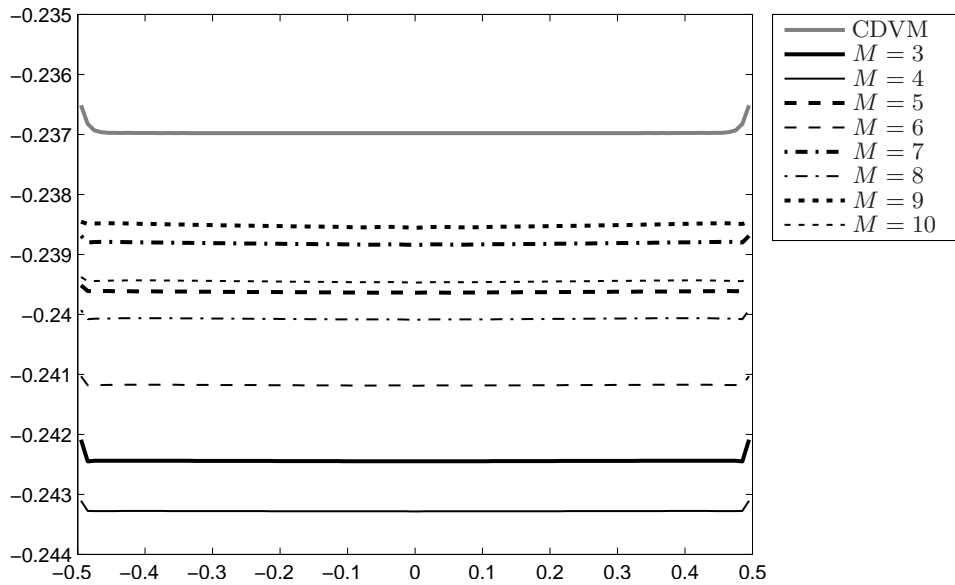
(a) Shear stress, σ_{12}
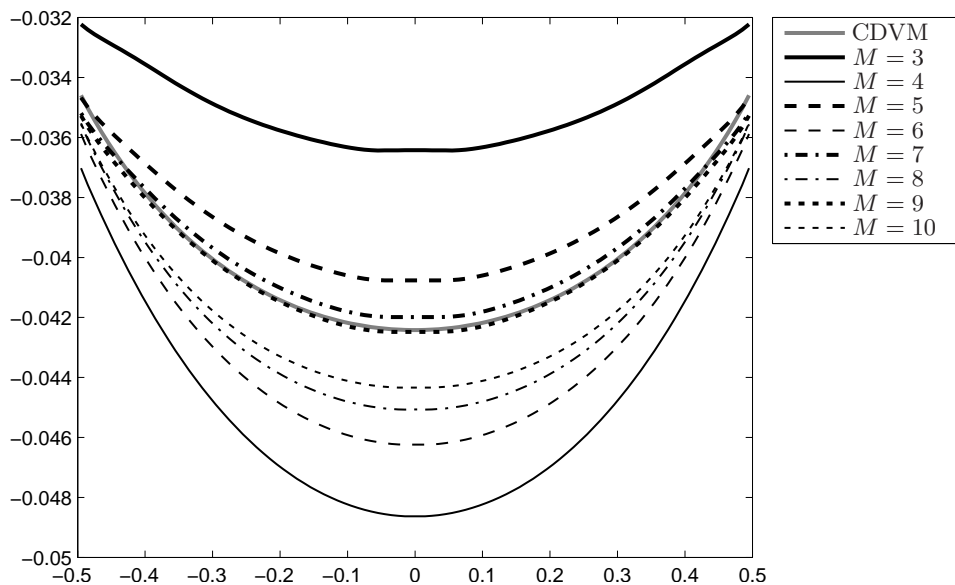
(b) Normal stress, σ_{22}

Figure 6: Shear and normal stress plots for the planar Couette flow with $Kn = 0.5$

variable while investigating the accuracy of moment equations. In this case, if we consider a steady state problem, the small parameter no longer appears in the governing equations (3.13). This means the order of magnitude for f_α does not increase as $|\alpha|$ increases, as has been found in [23].
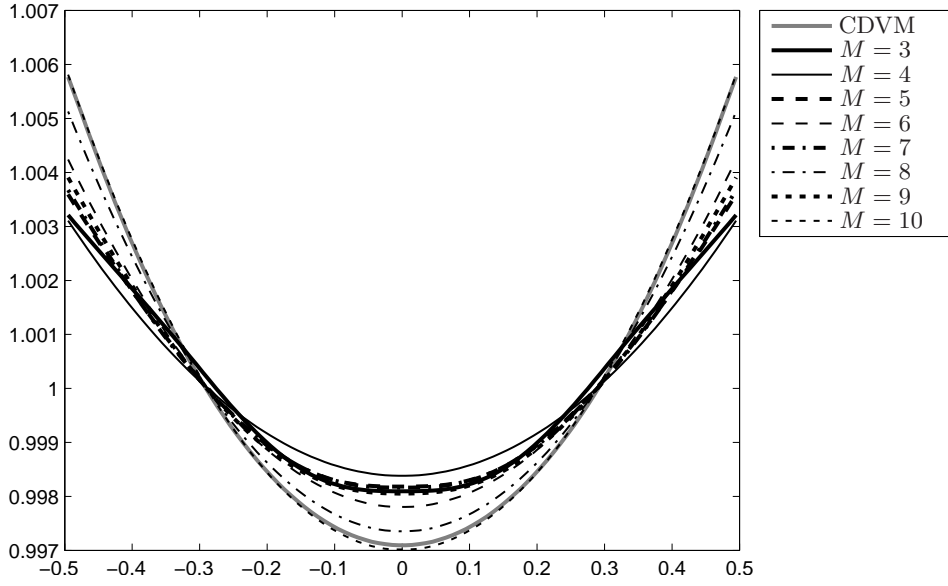
(a) Density, ρ
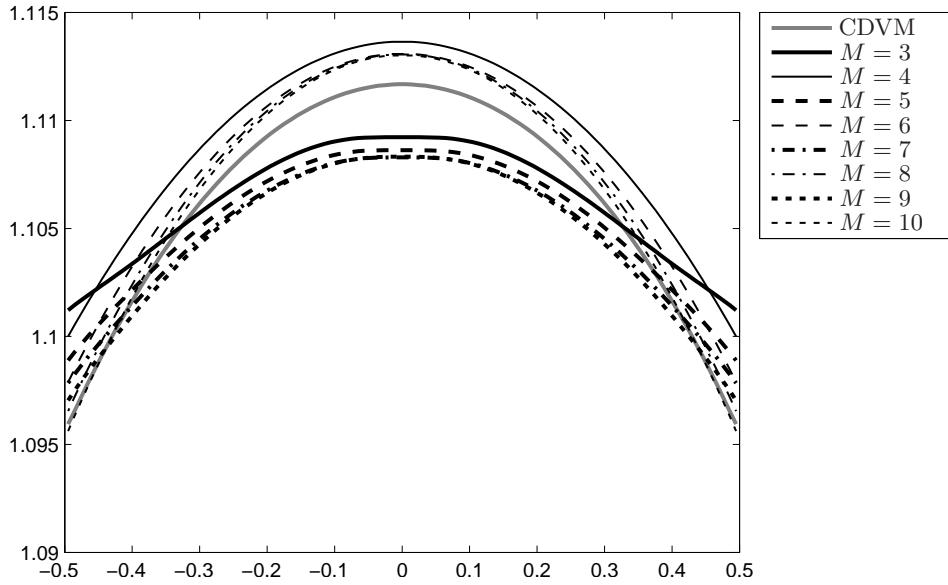
(b) Temperature, θ

Figure 7: Density and temperature plots for the planar Couette flow with $Kn = 1.0$

6.2 The validity of NRxx method for large Knudsen number and in the Knudsen layer

As we have discussed above, there are two cases when the order of accuracy is not so meaningful for describing the accuracy of the NRxx method:

1. In the case of $Kn \sim O(1)$, there are no "small parameters" in our concept.

2. In the Knudsen layer, the orders of magnitude of moments do not increase as they behave in the bulk.
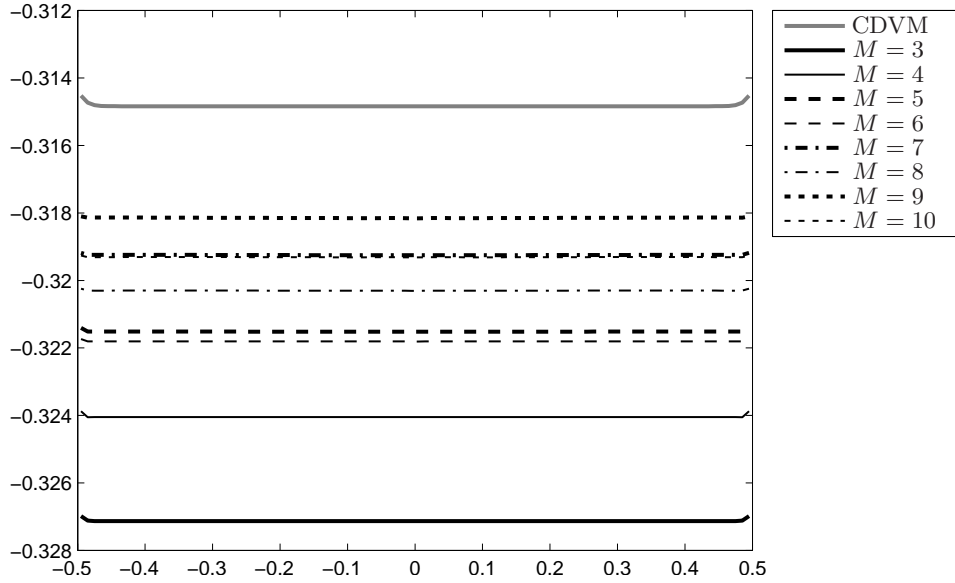
(a) Shear stress, σ_{12}
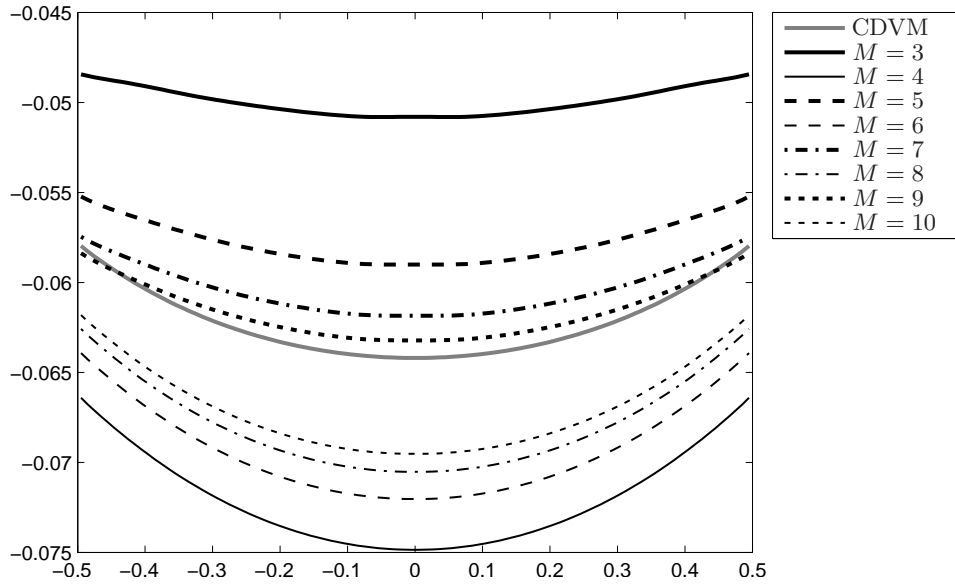
(b) Normal stress, σ_{22}

Figure 8: Shear and normal stress plots for the planar Couette flow with $Kn = 1.0$

Nevertheless, we can still consider the NRxx method as a solver for Boltzmann equation with spectral expansion in the velocity space, and the method should be valid when f_α decays sufficiently fast as $|\alpha|$ increases. Now we follow [23] and give the average absolute values of the moments with the same order for different Kn and different M in Figure 11. The result is based on the Couette flow problem in Section 5.2, and the NRxx solution at $x = -0.5$ is used in the these plots.

In these figures, we find that even when the Knudsen number is as large as 10, the magnitudes of moments still decay very fast. Thus, the NRxx method can still be considered to be valid and efficient. Although the methodology of regularization which is based
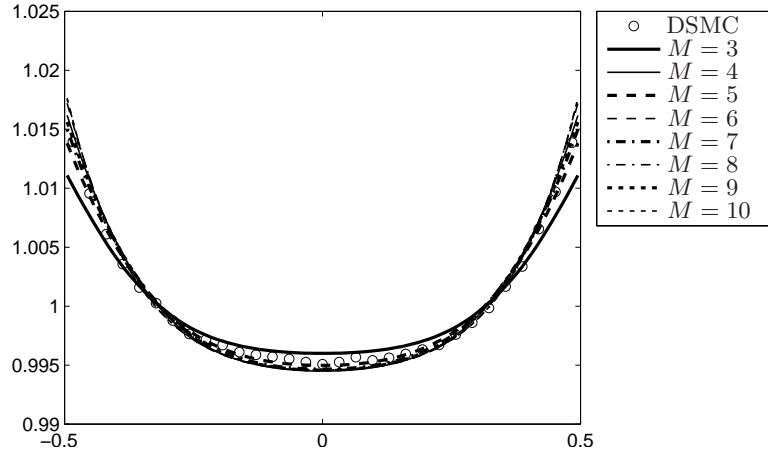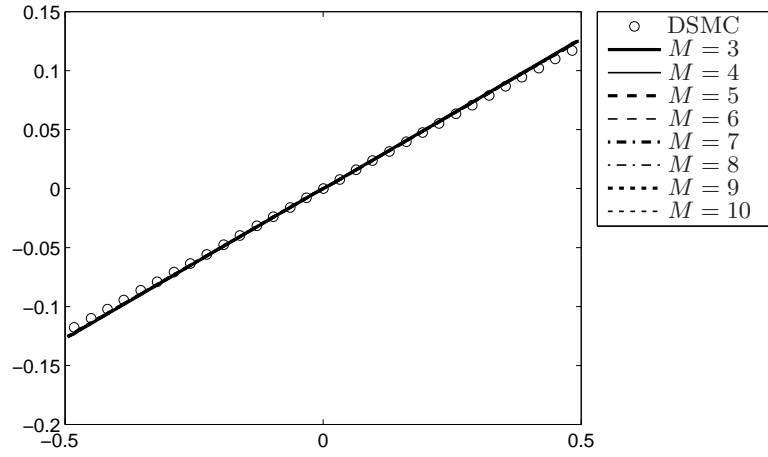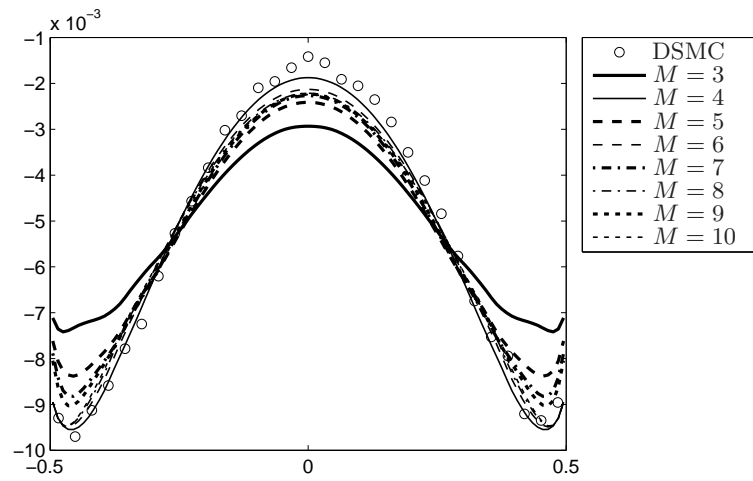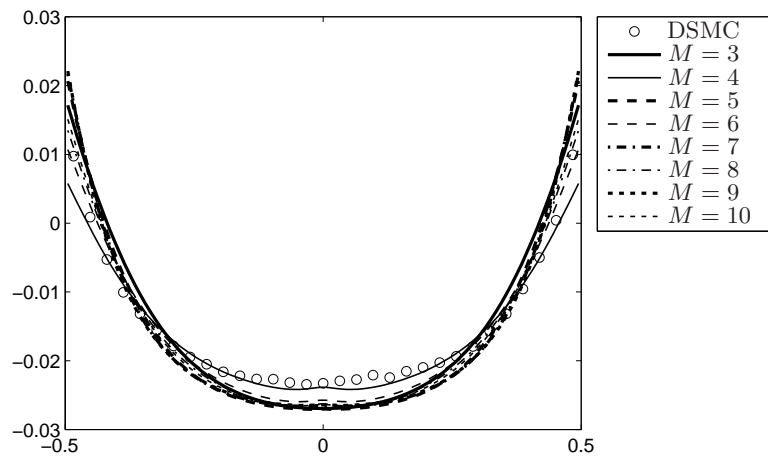
(a) Density, ρ
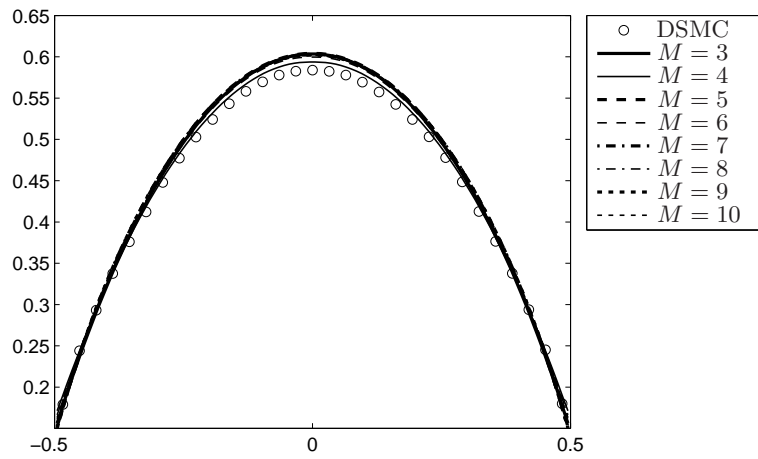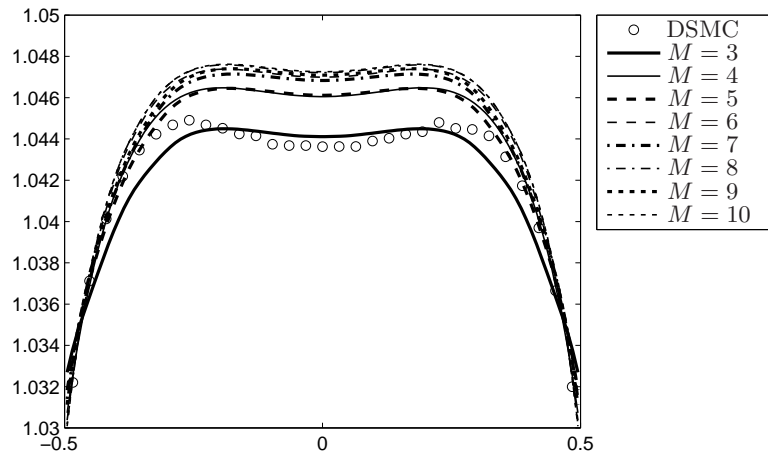
(b) Velocity, u_2

(c) Temperature, θ

Figure 9: Density, velocity and temperature plots for the planar Poiseuille flow

(a) Shear stress, σ_{12}

(b) Normal stress, σ_{22}

(c) Heat flux, q_1

Figure 10: Stress and heat flux plots for the planar Poiseuille flow

27

on a small τ is not valid any more, the regularization term (2.11) is simply a prediction of higher order moments. Such prediction differs from Grad equations' guess $f_\alpha = 0$, but also has a uniform expression for all Knudsen numbers. When M goes to infinity, the regularization term is expected to vanish since f_α decays. On the other hand, this term smooths the profiles of the macroscopic variables, thus avoids the appearance of some unphysical phenomena such as subshocks (see [5]). This indicates the meaningfulness of regularization for practical use.

7   Concluding remarks

A uniform numerical scheme for coupling the NRxx method and the wall boundary conditions are developed in this paper, and the NRxx method is extended to apply the force term and predict correct Prandtl number by using the Shakhov collision model. To validate the proposed method, both steady and unsteady problems are simulated. We are currently working on applying the NRxx method to 2D problems.

Acknowledgements

Appendix

A   Some properties of Hermite polynomials

The Hermite polynomials defined in (2.8) are a set of orthogonal polynomials over the domain $(-\infty, +\infty)$. Their properties can be found in many mathematical handbooks such as [1]. Some useful ones are listed below:

1. Orthogonality: $\int_{\mathbb{R}} He_m(x) He_n(x) \exp(-x^2/2)\, \mathrm{d}x = m! \sqrt{2\pi} \delta_{m,n}$;

2. Recursion relation: $He_{n+1}(x) = x He_n(x) - n He_{n-1}(x)$;

3. Differential relation: $He_n'(x) = n He_{n-1}(x)$.

And the following equality can be derived from the last two relations:

$$[He_n(x) \exp(-x^2/2)]' = -He_{n+1}(x) \exp(-x^2/2). \qquad (A.1)$$

B   Calculation of half-space integration

The detailed calculation of $I_{\alpha,\beta}(\theta)$ (4.9) will be presented. Using the definition of $\mathcal{H}_{\theta,\alpha}(\boldsymbol{v})$ (2.7), eq. (4.9) can be rewritten as

$$I_{\alpha,\beta}(\theta) = \prod_{k=1}^{3}\left[\frac{(2\pi)^{-1/2}}{\alpha_k!}\theta^{\frac{\alpha_k-\beta_k}{2}}\int_{l_k}^{+\infty}He_{\alpha_k}(v_k)He_{\beta_k}(v_k)\exp\left(-\frac{|v_k|^2}{2}\right)\mathrm{d}v_k\right], \qquad \text{(B.1)}$$

where

$$l_k = \begin{cases} -\infty, & k = 1,3, \\ 0, & k = 2. \end{cases} \qquad \text{(B.2)}$$

Applying the orthogonality of Hermite polynomials to (B.1), we have

$$I_{\alpha,\beta}(\theta) = \left[\frac{(2\pi)^{-1/2}}{\alpha_2!}\theta^{\frac{\alpha_2-\beta_2}{2}}\int_0^{+\infty}He_{\alpha_2}(v_2)He_{\beta_2}(v_2)\exp\left(-\frac{|v_2|^2}{2}\right)\mathrm{d}v_2\right]\cdot\delta_{\alpha_1\beta_1}\delta_{\alpha_3\beta_3}, \quad \text{(B.3)}$$

Now it is obvious that (4.10) holds if

$$S(m,n) = \frac{1}{\sqrt{2\pi}m!}\int_0^{+\infty}He_m(x)He_n(x)\exp(-x^2/2)\,\mathrm{d}x. \qquad \text{(B.4)}$$

Some simple cases can be directly worked out as

$$S(0,0) = \frac{1}{\sqrt{2\pi}}\int_0^{+\infty}\exp(-x^2/2)\,\mathrm{d}x = 1/2,$$

$$S(0,n) = \frac{1}{\sqrt{2\pi}}\int_0^{+\infty}He_n(x)\exp(-x^2/2)\,\mathrm{d}x = \frac{1}{\sqrt{2\pi}}He_{n-1}(0), \quad n \neq 0, \qquad \text{(B.5)}$$

$$S(m,0) = \frac{1}{\sqrt{2\pi}m!}\int_0^{+\infty}He_m(x)\exp(-x^2/2)\,\mathrm{d}x = \frac{1}{\sqrt{2\pi}m!}He_{m-1}(0), \quad m \neq 0.$$

This agrees with the first three cases of (4.11). For $m \neq 0$ and $n \neq 0$, we use the differential relation of Hermite polynomials and get

$$\begin{aligned}
S(m,n) &= -\frac{1}{\sqrt{2\pi}m!}\int_{x\in[0,+\infty)}He_n(x)\,\mathrm{d}[He_{m-1}(x)\exp(-x^2/2)] \\
&= \frac{1}{\sqrt{2\pi}m!}\left[He_{m-1}(0)He_n(0) + n\int_0^{+\infty}He_{m-1}(x)He_{n-1}(x)\exp(-x^2/2)\,\mathrm{d}x\right] \\
&= \frac{1}{\sqrt{2\pi}m!}He_{m-1}(0)He_n(0) + n/m\cdot S(m-1,n-1).
\end{aligned}$$

$$\text{(B.6)}$$

This is the last case in (4.11).

C   Expansion of the half-Maxwellian

This section is devoted to the detailed calculation of p_α defined in (4.23). Due to (4.26), only (4.24) and (4.25) need to be evaluated. We first consider $J_s(x)$ with $s \geqslant 1$.

By applying the recursion relation of Hermite polynomials, we get

$$
\begin{aligned}
J_s(x) &= \frac{1}{s!}\theta^{\frac{s+1}{2}} \int_{-\infty}^{+\infty} \frac{1}{\sqrt{2\pi\theta^W}} \exp\left(-\frac{|\sqrt{\theta}y - x|^2}{2\theta^W}\right) [yHe_{s-1}(y) - (s-1)He_{s-2}(y)]\,\mathrm{d}y \\
&= -\frac{\theta}{s}J_{s-2}(x) + \frac{x}{s}J_{s-1}(x) \\
&\quad + \underline{\frac{\theta^W}{s!}\theta^{\frac{s-1}{2}} \int_{-\infty}^{+\infty} \frac{1}{\sqrt{2\pi\theta^W}} \exp\left(-\frac{|\sqrt{\theta}y - x|^2}{2\theta^W}\right)\left(\frac{\theta}{\theta^W}y - \frac{x}{\theta^W}\sqrt{\theta}\right) He_{s-1}(y)\,\mathrm{d}y.}
\end{aligned}
\tag{C.1}
$$

For the underlined term, we use integration by parts and the differential relation of Hermite polynomials, and get

$$
\begin{aligned}
J_s(x) &= -\frac{\theta}{s}J_{s-2}(x) + \frac{x}{s}J_{s-1}(x) \\
&\quad + \frac{\theta^W}{s} \cdot \frac{1}{(s-2)!}\theta^{\frac{s-1}{2}} \int_{-\infty}^{+\infty} \frac{1}{\sqrt{2\pi\theta^W}} \exp\left(-\frac{|\sqrt{\theta}y - x|^2}{2\theta^W}\right) He_{s-2}(y)\,\mathrm{d}y \\
&= \frac{1}{s}\left[(\theta^W - \theta)J_{s-2}(x) + xJ_{s-1}(x)\right].
\end{aligned}
\tag{C.2}
$$

When $s = 0$ or $s = -1$, the integral (4.27) can be directly worked out as (4.30) since $He_0(y) \equiv 1$ and $He_{-1}(y) \equiv 0$.

The calculation of (4.25) is almost the same as (4.24). The only difference is that a boundary term will appear when integrating by parts. So the result becomes

$$
\tilde{J}_s(x) = \frac{1}{s}\left[(\theta^W - \theta)\tilde{J}_{s-2}(x) + x\tilde{J}_{s-1}(x)\right] - \frac{1}{s!}\sqrt{\frac{\theta^W}{2\pi}}\theta^{\frac{s-1}{2}} He_{s-1}(0) \exp\left(-\frac{x^2}{2\theta^W}\right), \quad s \geqslant 1
\tag{C.3}
$$

with initial conditions (4.31). Define

$$
H_s(x) = \frac{1}{s!}\sqrt{\frac{\theta^W}{2\pi}}\theta^{\frac{s-1}{2}} He_{s-1}(0) \exp\left(-\frac{x^2}{2\theta^W}\right).
\tag{C.4}
$$

Then (4.28) and (4.32) are natural. For $s \geqslant 1$, the recursion relation of H_s can be deduced as

$$
\begin{aligned}
H_s(x) &= \frac{\theta}{s(s-1)} \cdot \frac{1}{(s-2)!}\sqrt{\frac{\theta^W}{2\pi}}\theta^{\frac{s-3}{2}} [0 \cdot He_{s-2}(0) - (s-2)He_{s-3}(0)] \exp\left(-\frac{x^2}{2\theta^W}\right) \\
&= -\frac{s-2}{s(s-1)}\theta H_{s-2}(x).
\end{aligned}
\tag{C.5}
$$

References

[1] M. Abramowitz and I. A. Stegun. *Handbook of Mathematical Functions with Formulas, Graphs, and Mathematical Tables.* Dover, New York, 1964.

[2] P. L. Bhatnagar, E. P. Gross, and M. Krook. A model for collision processes in gases. I. small amplitude processes in charged and neutral one-component systems. *Phys. Rev.*, 94(3):511–525, 1954.

[3] G. A. Bird. *Molecular Gas Dynamics and the Direct Simulation of Gas Flows*. Oxford: Clarendon Press, 1994.

[4] Z. Cai and R. Li. Numerical regularized moment method of arbitrary order for Boltzmann-BGK equation. *SIAM J. Sci. Comput.*, 32(5):2875–2907, 2010.

[5] Z. Cai, R. Li, and Y. Wang. Numerical regularized moment method for high Mach number flow. To appear in *Commun. Comput. Phys.*

[6] Z. Cai, R. Li, and Y. Wang. An efficient NRxx method for Boltzmann-BGK equation. *J. Sci. Comput.*, 2011. DOI: 10.1007/s10915-011-9475-5.

[7] H. Grad. On the kinetic theory of rarefied gases. *Comm. Pure Appl. Math.*, 2(4):331–407, 1949.

[8] H. Grad. The profile of a steady plane shock wave. *Comm. Pure Appl. Math.*, 5(3):257–300, 1952.

[9] H. Grad. Principles of the kinetic theory of gases. *Handbuch der Physik*, 12:205–294, 1958.

[10] X. J. Gu and D. R. Emerson. A computational strategy for the regularized 13 moment equations with enhanced wall-boundary equations. *J. Comput. Phys.*, 255(1):263–283, 2007.

[11] X. J. Gu and D. R. Emerson. A high-order moment approach for capturing non-equilibrium phenomena in the transition regime. *J. Fluid Mech.*, 636:177–216, 2009.

[12] S. Jin and M. Slemrod. Regularization of the Burnett equations via relaxation. *J. Stat. Phys*, 103(5–6):1009–1033, 2001.

[13] G. Karniadakis, Ali Beskok, and Narayan Aluru. *Microflows and Nanoflows: Fundamentals and Simulation*, volume 29 of *Interdisciplinary Applied Mathematics*. Springer, New York, U.S.A., 2005.

[14] A. N. Kudryavtsev, A. A. Shershnev, and M. S. Ivanov. Comparison of different kinetic and continuum models applied to the shock-wave structure problem. In T. Abe, editor, *Rarefied Gas Dynamics: 26th International Symposium*, volume 1084, pages 507–512. AIP, 2008.

[15] J. Clerk Maxwell. On stresses in rarefied gases arising from inequalities of temperature. *Proc. R. Soc. Lond.*, 27(185–189):304–308, 1878.

[16] S. Mizzi, X. J. Gu, D. R. Emerson, R. W. Barber, and J. M. Reese. Computational framework for the regularized 20-moment equations for non-equilibrium gas flows. *Int. J. Num. Meth. Fluids*, 56(8):1433–1439, 2008.

[17] I. Müller, D. Reitebuch, and W. Weiss. Extended thermodynamics – consistent in order of magnitude. *Continuum Mech. Thermodyn.*, 15(2):113–146, 2002.

[18] D. Reitebuch and W. Weiss. Application of high moment theory to the plane Couette flow. *Continuum Mech. Thermodyn.*, 11(4):217–225, 1999.

[19] E. M. Shakhov. Generalization of the Krook kinetic relaxation equation. *Fluid Dyn.*, 3(5):95–96, 1968.

[20] H. Struchtrup. Kinetic schemes and boundary conditions for moment equations. *Z. Angew. Math. Phys.*, 51(3):346–365, 2000.

[21] H. Struchtrup. Grad's moment equations for microscale flows. In A. D. Ketsdever and E. P. Muntz, editors, *Rarefied Gas Dynamics: 23rd International Symposium*, volume 663, pages 792–799. AIP, 2003.

[22] H. Struchtrup. *Macroscopic Transport Equations for Rarefied Gas Flows: Approximation Methods in Kinetic Theory.* Springer, 2005.

[23] H. Struchtrup. Linear kinetic heat transfer: moment equations, boundary conditions, and Knudsen layers. *Physica A*, 387(8–9):1750–1766, 2008.

[24] H. Struchtrup and M. Torrilhon. Regularization of Grad's 13 moment equations: Derivation and linear analysis. *Phys. Fluids*, 15(9):2668–2680, 2003.

[25] P. L. Tallec and J. P. Perlat. Numerical analysis of Levermore's moment system. Rapport de recherche 3124, INRIA Rocquencourt, March 1997.

[26] T. Thatcher, Y. Zheng, and H. Struchtrup. Boundary conditions for Grad's 13 moment equations. *Progress Comput. Fluid Dyn.*, 8(1–4):69–83, 2008.

[27] V. A. Titarev. Numerical method for computing two-dimensional unsteady rarefied gas flows in arbitrarily shaped domains. *Comput. Math. Math. Phys.*, 49(7):1197–1211, 2009.

[28] M. Torrilhon and H. Struchtrup. Boundary conditions for regularized 13-moment-equations for micro-channel-flows. *J. Comput. Phys.*, 227(3):1982–2011, 2008.

[29] W. Weiss. Continuous shock structure in extended thermodynamics. *Phys. Rev. E*, 52(6):R5760–R5763, 1995.

[30] K. Xu, H. Liu, and J. Jiang. Multiple-temperature model for continuum and near continuum flows. *Phys. Fluids*, 19(1):016101, 2007.

[31] J. Y. Yang and J. C. Huang. Rarefied flow computations using nonlinear model Boltzmann equations. *J. Comput. Phys.*, 120(2):323–339, 1995.

[32] Y. Zheng and B. J. Alder A. L. Garcia. Comparison of kinetic theory and hydrodynamics for Poiseuille flow. *J. Stat. Phys.*, 109(3–4):495–505, 2002.
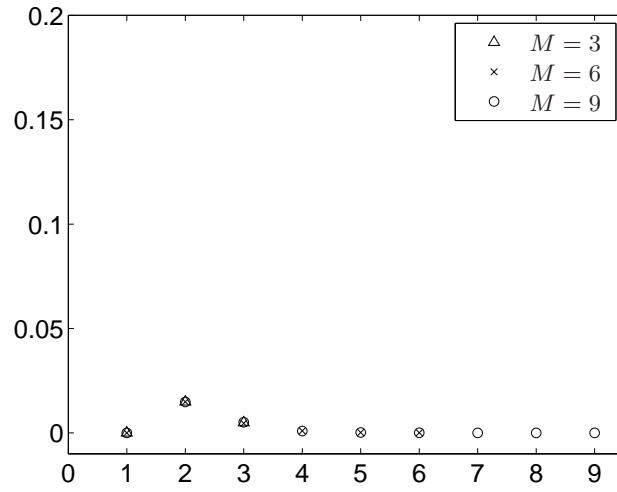
(a) $Kn = 0.1$
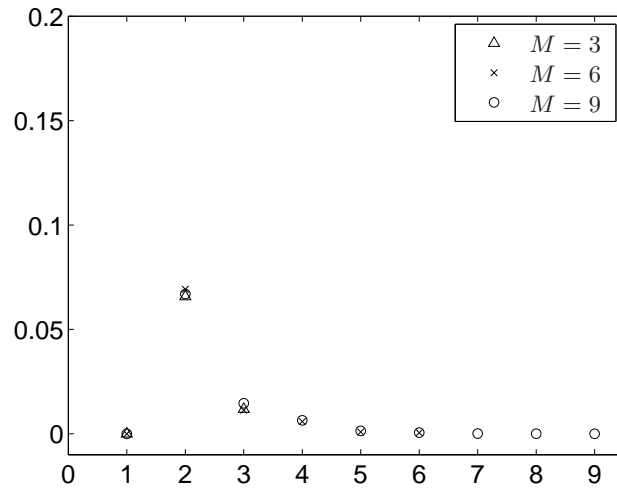
(b) $Kn = 1.0$
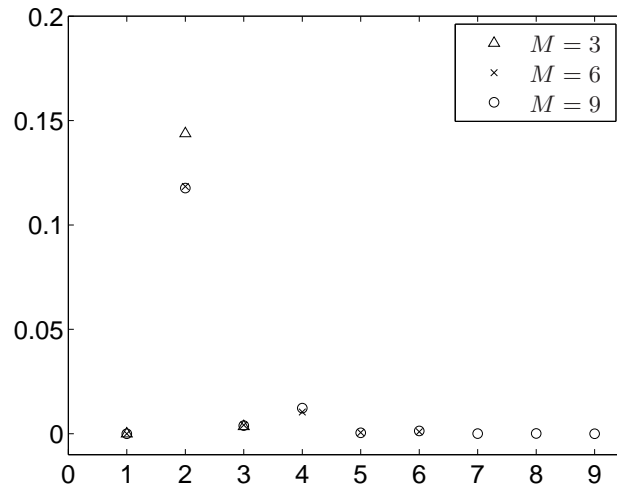
(c) $Kn = 10.0$

Figure 11: Average values of $\{|f_\alpha|\}_{|\alpha|=k}$ for $k = 1$ to 9. The results are based the NRxx solutions of the Couette flow.